The Astrophysical Journal, 788:28 (19pp), 2014 June 10 doi:10.1088/0004-637X/788/1/28

3D-HST+CANDELS: THE EVOLUTION OF THE GALAXY SIZE–MASS DISTRIBUTION SINCE $z = 3$

A. van der Wel[1], M. Franx[2], P. G. van Dokkum[3], R. E. Skelton[4], I. G. Momcheva[3], K. E. Whitaker[5], G. B. Brammer[6], E. F. Bell[7], H.-W. Rix[1], S. Wuyts[8], H. C. Ferguson[6], B. P. Holden[9], G. Barro[9], A. M. Koekemoer[6], Yu-Yen Chang[1], E. J. McGrath[10], B. Häussler[11,12], A. Dekel[13], P. Behroozi[6], M. Fumagalli[2], J. Leja[3], B. F. Lundgren[14], M. V. Maseda[1], E. J. Nelson[3], D. A. Wake[14,15], S. G. Patel[16], I. Labbé[2], S. M. Faber[9], N. A. Grogin[6], and D. D. Kocevski[17]
[1] Max-Planck Institut für Astronomie, Königstuhl 17, D-69117 Heidelberg, Germany; e-mail: vdwel@mpia.de
[2] Leiden Observatory, Leiden University, P.O. Box 9513, NL-2300 AA Leiden, The Netherlands
[3] Department of Astronomy, Yale University, New Haven, CT 06511, USA
[4] South African Astronomical Observatory, P.O. Box 9, Observatory 7935, South Africa
[5] Astrophysics Science Division, Goddard Space Center, Greenbelt, MD 20771, USA
[6] Space Telescope Science Institute, 3700 San Martin Drive, Baltimore, MD 21218, USA
[7] Department of Astronomy, University of Michigan, 500 Church Street, Ann Arbor, MI 48109, USA
[8] Max-Planck Institut für Extraterrestrische Physik, Giessenbachstrasse, D-85748 Garching, Germany
[9] University of California Observatories/Lick Observatory, University of California, Santa Cruz, CA 95064, USA
[10] Department of Physics and Astronomy, Colby College, Waterville, ME 0490, USA
[11] Physics Department, University of Oxford, Denys Wilkinson Building, Keble Road, Oxford OX1 3RH, UK
[12] Centre for Astrophysics, Science & Technology Research Institute, University of Hertfordshire, Hatfield, Herts AL10 9AB, UK
[13] Racah Institute of Physics, The Hebrew University, Jerusalem 91904, Israel
[14] Department of Astronomy, University of Wisconsin, Madison, WI 53706, USA
[15] The Department of Physical Sciences, The Open University, Milton Keynes MK7 6AA, UK
[16] Observatories of the Carnegie Institution of Washington, Pasadena, CA 91101, USA
[17] Department of Physics and Astronomy, University of Kentucky, Lexington, KY 40506, USA
Received 2014 March 3; accepted 2014 April 9; published 2014 May 19

ABSTRACT

Spectroscopic + photometric redshifts, stellar mass estimates, and rest-frame colors from the 3D-HST survey are combined with structural parameter measurements from CANDELS imaging to determine the galaxy size–mass distribution over the redshift range $0 < z < 3$. Separating early- and late-type galaxies on the basis of star-formation activity, we confirm that early-type galaxies are on average smaller than late-type galaxies at all redshifts, and we find a significantly different rate of average size evolution at fixed galaxy mass, with fast evolution for the early-type population, $R_{\rm eff} \propto (1+z)^{-1.48}$, and moderate evolution for the late-type population, $R_{\rm eff} \propto (1+z)^{-0.75}$. The large sample size and dynamic range in both galaxy mass and redshift, in combination with the high fidelity of our measurements due to the extensive use of spectroscopic data, not only fortify previous results but also enable us to probe beyond simple average galaxy size measurements. At all redshifts the slope of the size–mass relation is shallow, $R_{\rm eff} \propto M_*^{0.22}$, for late-type galaxies with stellar mass $>3 \times 10^9\,M_\odot$, and steep, $R_{\rm eff} \propto M_*^{0.75}$, for early-type galaxies with stellar mass $>2 \times 10^{10}\,M_\odot$. The intrinsic scatter is $\lesssim$0.2 dex for all galaxy types and redshifts. For late-type galaxies, the logarithmic size distribution is not symmetric but is skewed toward small sizes: at all redshifts and masses, a tail of small late-type galaxies exists that overlaps in size with the early-type galaxy population. The number density of massive ($\sim 10^{11}\,M_\odot$), compact ($R_{\rm eff} < 2$ kpc) early-type galaxies increases from $z = 3$ to $z = 1.5$–2 and then strongly decreases at later cosmic times.

Key words: galaxies: evolution – galaxies: fundamental parameters – galaxies: high-redshift – galaxies: structure

Online-only material: color figures

1. INTRODUCTION

The size distribution of the stellar bodies of galaxies, and its evolution with cosmic time, provides important clues about the assembly history of galaxies and the relationship with their dark matter halos. The two main classes of galaxies, early and late types, show very different dependencies between size and stellar mass (Shen et al. 2003). The weak dependence between size and mass for late-type galaxies implies that the high-mass late types, on average, have higher surface mass densities than low-mass late types. In contrast, early types show a more complex relationship between stellar mass and density, with the density peaking for systems with stellar masses around $M_* \sim 4 \times 10^{10} M_\odot$ and decreasing toward both lower and higher masses, as reflected in the classical Kormendy (1977) relation. This fundamental difference does not depend on whether classification of early and late types is based on star formation activity, bulge dominance (Sérsic index), or visual inspection, and it implies that the two types have very different evolutionary and assembly histories.

In this paper we present the evolution of the size–mass distribution up to $z = 3$ on the basis of spectroscopy and multiwavelength photometry from the 3D-HST survey (Brammer et al. 2012) and *HST*/WFC3 imaging from CANDELS (Grogin et al. 2011; Koekemoer et al. 2011). Angular galaxy sizes are measured from the CANDELS imaging as described by van der Wel et al. (2012), and the *HST*/WFC3 grism observations from 3D-HST provide spectroscopic confirmation and redshifts for a large fraction of the sample, considerably strengthening—with respect to previous studies—the fidelity of estimates for stellar masses and rest-frame photometric properties.

So far, most of the previous studies have focused on the evolution of average galaxy sizes of the high-mass end of the

distribution ($\gtrsim 5 \times 10^{10}\,M_{\odot}$). Enabled by both the improved data quality and a five-fold increase in sample size, we can now, for the first time, describe the size distribution of galaxies across redshift.

1.1. Size Evolution of Late-type Galaxies

Tracing the evolution of the size distribution with redshift allows us to test the most basic elements in our theory of galaxy formation. The zeroth-order expectation is that disk scale lengths evolve fast, approximately as the inverse of the Hubble parameter (Mo et al. 1998), and early and recent work on the average sizes of Lyman break galaxies (LBGs) at high redshifts ($z \sim 2$–6) roughly agree with this expectation for a ΛCDM cosmology: Giavalisco et al. (1996), Ferguson et al. (2004), Oesch et al. (2010), and Mosleh et al. (2012) all find rapid size evolution with redshift, $R_{\rm eff} \propto (1+z)^{\beta=-1.1}$.

In contrast, the average size of the population of disk-dominated galaxies at late times ($z \lesssim 1$) has been reported to evolve slowly or not at all (Lilly et al. 1998; Ravindranath et al. 2004; Barden et al. 2005). The implication would be that the evolution of the disk galaxy population is decoupled from the evolution of the dark matter halo population. One fundamental difference between the results of LBGs and lower-redshift disk galaxies is the rest-frame wavelength at which the sizes are measured: the rest-frame UV light seen for LBGs originates from young stars that may be, and are generally expected to be, distributed differently than the bulk of baryonic and stellar mass, not to mention the consequences of extinction.

The advent of ground-based near-infrared imaging surveys helped to bridge the $z < 1$ and $z > 2$ regimes by enabling size measurements in a consistent manner at a fixed rest-frame wavelength. Early results suggested slow evolution for late-type galaxies up to $z \sim 3$ (Trujillo et al. 2006a), but the uncertainties at $z > 1$ were such that evolution in that regime was not strongly constrained. Later ground-based work pointed at faster evolution at a fixed galaxy mass: Franx et al. (2008) found $\beta = -0.6$ and Williams et al. (2010) found $\beta = -0.9$, but precise constraints at $z > 1.5$ remained elusive and the apparent tension between the $z \lesssim 1$ work and the near-infrared at $z \sim 1.5$ unaddressed.

Several *HST*/NICMOS-based studies of the morphology and structure of massive $z \sim 2$ galaxies in the rest-frame optical eventually led to mostly converged results, with $\beta \sim -0.8$ for massive ($\sim 10^{11}\,M_{\odot}$) star-forming galaxies from $z \sim 2.5$ to the present (Toft et al. 2007; Buitrago et al. 2008; Kriek et al. 2009a). So far it has remained unclear as to whether the difference with the significantly faster evolution for LBG galaxies ($\beta \sim -1.1$) is caused by morphological K corrections, the difference in mass (the typical LBG has $M_{*} \sim 10^{10}\,M_{\odot}$), or physical changes with redshift. In addition, the difference with the previously mentioned studies at $z < 1$ (Lilly et al. 1998; Ravindranath et al. 2004; Barden et al. 2005) remains unexplained.

Improving the measurement of β and its mass dependence is crucial in order to take the next step toward understanding disk galaxy formation. In this paper we will address these issues and describe the full size–mass distribution of high-redshift galaxies over a broad range in galaxy mass and redshift. We will

1. measure the evolution of the slope of the size–mass relation;
2. present the size distribution as a function of stellar mass and redshift;
3. provide a consistent comparison with UV-selected, high-redshift samples.

1.2. Size Evolution of Early-type Galaxies

Over the past five years, more attention has been bestowed on the size evolution of early-type galaxies than on the size evolution of late-type star-forming galaxies. Interest in the topic was initiated by reports that $z \sim 1.5$ early-type galaxies have remarkably small sizes in *Hubble Space Telescope* (*HST*)-based rest-frame UV imaging (Daddi et al. 2005; Trujillo et al. 2007) and ground-based near-infrared imaging (Trujillo et al. 2006b). NICMOS imaging presented by Zirm (2007), Toft et al. (2007), Stockton et al. (2008), and McGrath et al. (2008) provided space-based rest-frame optical size measurements that strengthened the evidence for rapid size evolution ($\beta = -1$ or faster) as measured at a fixed galaxy mass ($\sim 10^{11}\,M_{\odot}$). This notion became firmly established through larger samples (Buitrago et al. 2008) and the first spectroscopic samples (van Dokkum et al. 2008; Damjanov et al. 2011).

Concerns regarding gross overestimates of the stellar mass content of the compact early-type galaxies were alleviated by dynamical mass estimates of such galaxies at $z \gtrsim 1$ (van der Wel et al. 2008; Cimatti et al. 2008; Newman et al. 2010; van de Sande et al. 2011; Toft et al. 2012; van de Sande et al. 2013; Bezanson et al. 2013; Belli et al. 2014), and the analysis by Szomoru et al. (2010) of ultra-deep imaging of a single compact galaxy has demonstrated the absence of low-surface brightness wings that could have been missed by shallower imaging. Increases in sample size and dynamic range in stellar mass have constrained the average size evolution of early-type galaxies with stellar masses $>5 \times 10^{10}\,M_{\odot}$ to $\beta \sim -1.3$ up to $z = 2.5$, with no evidence for a change in the slope of the relation over this mass range (Newman et al. 2012). The steepness of the relation combined with the non-negligible scatter accommodates observations that early-type galaxies display a large range in size at $z > 1$ (e.g., Mancini et al. 2010; Saracco et al. 2011).

While the observational results have largely converged, the interpretation is still debated. Some authors have considered the average increase in size over time as being due to the addition of new, larger early-type galaxies. While some argue that this cannot reproduce the observations (van der Wel et al. 2009a), others argue that a population of compact early-type galaxies (with sizes $R_{\rm eff} \lesssim 2$ kpc) exists within present-day clusters, with a number density comparable to that of higher-redshift early-type galaxies (Valentinuzzi et al. 2010; Poggianti et al. 2013); tension with the absence of such galaxies in the Sloan Digital Sky Survey (SDSS) remains (Trujillo et al. 2009; Taylor et al. 2010). The crucial observational test is to trace the evolution of the number density of early-type galaxies as a function of their size. Cassata et al. (2011), Szomoru et al. (2012), and Newman et al. (2012) show strong evolution in the number density of small galaxies at $0 < z < 2.5$, while Carollo et al. (2013) claim no evolution at $0 < z < 1$. Our use of 5 fields addresses the issue of field-to-field variations that may affect the aforementioned studies based on smaller samples, and it extends the dynamic redshift range of the Carollo et al. sample.

The leading explanation for the size growth of individual galaxies is accretion and tidal disruption of satellite galaxies that gradually build up the outer parts. For this process, the change in size is large compared with the increase in mass: $\Delta R_{\rm eff} \propto \Delta M_{*}^{2}$ (e.g., Bezanson et al. 2009; Hopkins et al. 2009). This analytical prediction based on conservation of binding energy has been tested through numerical simulations (e.g., Naab et al. 2009; Oser et al. 2012; Bédorf & Portegies Zwart

2013). The analytically predicted and simulated evolution in the increased surface mass density at large radii is, in fact, observed (van Dokkum et al. 2010); in addition, the central stellar density shows little evolution (Bezanson et al. 2009; Hopkins et al. 2009; van Dokkum et al. 2010), which is also consistent with a minor merger scenario. In other words, the observations show that there is no need, and little room, to physically expand a galaxy by displacing large numbers of stars to large radii through rapid changes in the central potential, as suggested by Fan et al. (2010). A possible challenge to the minor merger scenario is posed by the lack of strong evolution in the slope of the mass density profile seen in lensing galaxies (Sonnenfeld et al. 2013).

Until recently, the size evolution of late- and early-type galaxies was usually discussed separately and treated as different topics. However, in order to understand the joint evolution of these classes, one has to take into account the continuous transition of late-type to early-type galaxies seen in particular in the stellar mass range of $10^{10}\,M_{\odot}$ to $10^{11}\,M_{\odot}$ (e.g., Bell et al. 2004; Faber et al. 2007; Brown et al. 2007; Ilbert et al. 2010; Brammer et al. 2011; Buitrago et al. 2013; Muzzin et al. 2013). The star-forming progenitors of the small early-type galaxies are now looked for and plausibly identified (e.g., Whitaker et al. 2011; Barro et al. 2013a, 2013b; Toft et al. 2014), but the evolutionary path of the transitioning galaxies has not been fully mapped out.

In this paper, regarding the evolution of early-type galaxies, we will

1. present the distribution of sizes as a function of stellar mass and redshift, jointly with those of late-type galaxies; and
2. show the evolution of the number density of early-type galaxies as a function of size.

After describing the data and sample selection in Section 2, we present and analyze size distributions as a function of redshift and galaxy mass in Section 3. We compare our results with previous studies in Section 4 and then discuss the implications of our findings in Section 5. We assume the cosmological parameters $(\Omega_{\rm M}, \Omega_{\Lambda}, h) = (0.27, 0.73, 0.71)$. Finally, we use AB magnitudes and the Chabrier (2003) stellar initial mass function.

2. DATA

The procedures for source detection, multiwavelength photometry, redshift determinations, rest-frame color, and stellar mass estimates are described elsewhere. Here we briefly summarize these steps.

2.1. Source Detection

The 207,967 sources in all five CANDELS/3D-HST fields (Koekemoer et al. 2011; Brammer et al. 2012) are detected in and extracted from images that combine the available *HST*/WFC3 IR channel data; that is, stacked mosaics consisting of F125W, F140W, and F160W imaging are constructed for this purpose. We refer to the photometry data release paper from the 3D-HST collaboration by Skelton et al. (2014) for details.

2.2. Photometric and Spectroscopic Redshift Determinations

Multiwavelength photometry from *HST*/WFC3 and *HST*/ACS imaging is produced by creating point-spread-function (PSF)-matched images, using custom-made kernels and performing simple aperture photometry. Multiwavelength photometry from ground-based optical-NIR and *Spitzer*/IRAC imaging is produced using the approach outlined by Labbé et al. (2006) and further developed by González et al. (2010), which addresses blending by nearby sources and takes the large differences in PSF into account through the use of custom-made convolution kernels. Like alternative methods such as TFIT (Laidler et al. 2007), our approach uses high-resolution images as priors to model sources in lower-resolution images.

Photometric redshifts are determined on the basis of the multiwavelength photometry using the EAZY package (Brammer et al. 2008). Skelton et al. (2014) describe the procedure in full, but it essentially follows Whitaker et al. (2011): briefly, linear combinations of a set of templates that span the range of observed galaxy properties are used to fit the photometry, producing a marginalized posterior probability distribution for the redshift, with $z_{\rm phot}$ as its peak.

The photometric redshifts provide a baseline for 3D-HST WFC3 G141 grism spectroscopy to provide more precise redshift information. Brammer et al. (2012) describe the extraction of spectra and redshift determination in detail. The method has been updated to use interlaced rather than drizzled *HST*/WFC3 mosaics, which are used to construct the photometric catalogs. For all sources brighter than $\mathrm{F160W_{AB}} = 23$, the F140W image is traced along the dispersed WFC3/G141 grism image, such that a spectrum is extracted that accounts for the convolved spectral and spatial information of the low wavelength resolution ($R \sim 130$) grism data.

For each extracted object, the spectroscopic information is combined with the photometric redshift probability distribution, producing a new best-fitting redshift (I. G. Momcheva et al., in preparation). Finally, spectroscopic redshifts from the literature are used when available.

The grism data significantly improve the redshift precision for thousands of galaxies and provide indispensable evidence for the good accuracy of the purely photometric redshift estimates. The current version of the 3D-HST redshift catalog contains grism redshift information for all objects brighter than $H_{\rm F160W} = 23$ and for which such data is available (∼75% of the CANDELS area). For our mass-limited sample—defined below in Section 2.4—this amounts to ∼10,000 galaxies. This is ∼30% of the total sample and 50% for the sample of massive ($M_* > 10^{10}\,M_{\odot}$) galaxies in the crucial redshift range $1 < z < 3$. For these galaxies the Quadri & Williams (2010) pair test demonstrates a precision of $\Delta z/(1+z) = 0.003$, or 0.3%. For purely photometric redshifts this is 1%–2.5%, depending on the varying photometric data set available for each of the five fields, suggesting a factor of 3–10 improvement in redshift precision from the grism data. There is no systematic offset between the two sets of redshifts.

2.3. Rest-frame Colors and Stellar Mass Estimates

EAZY is used to compute the rest-frame $U - V$ and $V - J$ colors, and the package FAST (Kriek et al. 2009b) is used to estimate stellar masses. A large number of Bruzual & Charlot (2003) templates with solar metallicity, a wide range in age (4×10^7 yr to 12.5×10^9 yr, but always younger than the universe), exponentially declining star-formation histories (with time scales $\tau = 10^7$–10^{10} yr), and dust extinction ($A_{\rm V} = 0$–4) are used and matched to the photometry. The final stellar mass is corrected for the difference between the total F160W flux from the photometric catalog and the total F160W as measured with GALFIT (see Section 2.5). F125W is used in case F160W is not available. This correction ensures that our size and mass estimates are mutually consistent in that both are based on the same model for the light distribution.

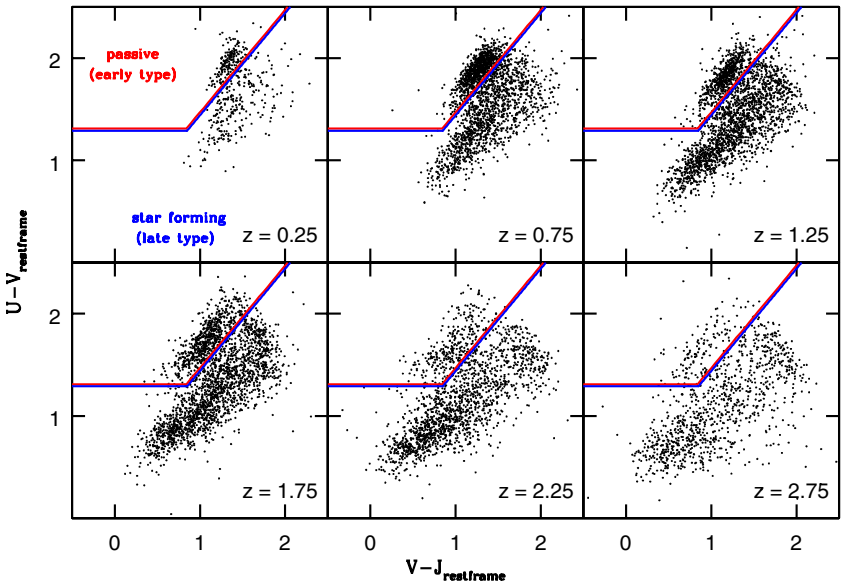

Figure 1. Rest-frame $U - V$ vs. $V - J$ color distribution for six redshift bins (each 0.5 wide). The two distinct classes of quiescent and star-forming galaxies are separated by the indicated selection criteria to define our early- and late-type galaxy samples.

(A color version of this figure is available in the online journal.)

The uncertainties in the stellar mass estimates can be large and are to some extent still unknown. However, the possible error in the mass-to-light ratio for low-mass blue galaxies with precisely known redshifts due to uncertainties in the star-formation history (SFH) and metallicity is not larger than a factor of a few. Moreover, for high-mass galaxies the relation between dynamical and stellar mass estimates is the same to within a factor of $\sim$2 over the whole redshift range $0 < z < 2$, indicating that stellar mass estimates are reasonably consistent at different redshifts (e.g., van der Wel et al. 2006; van de Sande et al. 2013). The direct mass measurement of a $z \sim 1.5$ strong gravitational lens is also in agreement with the photometrically estimated stellar mass (van der Wel et al. 2013). For these reasons we are confident that the analysis presented in this paper, which looks at galaxies that span several orders of magnitude in stellar mass, is not fundamentally dependent on the current uncertainties in the mass estimates.

2.4. Sample Selection

Following Wuyts et al. (2007) and Williams et al. (2009), we utilize rest-frame colors to distinguish between the two basic classes of galaxies: star-forming and quiescent galaxies. In this paper we refer to the former as late-type galaxies and to the latter as early-type galaxies. In Figure 1 we show the rest-frame $U - V$ and $V - J$ color distribution of galaxies with stellar mass in excess of $10^{10}\,M_{\odot}$ for a range of redshifts. Even beyond $z = 2$ the early- and late-type galaxies are separated in this space, which allows us to effectively assign each object to one of the two classes.

An indication of the high fidelity of this selection method is that less than 20% of the thus classified early-type galaxies with matches in the FIREWORKS catalog from Wuyts et al. (2007) are detected at 24 μm, while more than $\sim$80% of the late-type galaxies are detected—these numbers are for the mass range $3 \times 10^{10}\,M_{\odot} < M_{\odot} < 10^{11}\,M_{\odot}$ and the redshift range $1 < z < 2$. We note that a simpler selection by just $U - V$ color would compromise the separation into types, as the subsample of galaxies that are red in $U - V$ consist of dusty and quiescent objects. In addition, 80% of the color-selected early-type (late-type) galaxies have Sérsic indices large (smaller) than $n = 2.5$.

We adopt redshift- and color-dependent mass limits (Figure 2) that are set by the F160W magnitude limit down to which galaxy sizes—here described in Section 2.5—can be determined with high fidelity. van der Wel et al. (2012) showed that galaxy sizes can be precisely and accurately determined down to a magnitude limit of $H_{\rm F160W} = 24.5$; at fainter magnitudes the random and systematic errors can exceed 20% for large galaxies with large Sérsic indices. Since most $z > 1$ galaxies in our sample have small sizes (0.″3 in the median) and low Sérsic indices (1.4 in the median) this magnitude limit is conservative.

Out to $z = 3$ our magnitude-limited sample is complete in stellar mass down to $\sim 10^{10}\,M_{\odot}$ (see Figure 2). This limit is 1.9 magnitudes brighter than the 5σ detection limit, and simulations of artificial objects inserted in the images show that $\gtrsim$95% of all objects are detected (Skelton et al. 2014). Therefore, incompleteness will not be an issue for our sample, and biases against large (or small) galaxies will not play a significant role.

Our mass-selected sample, with a redshift-dependent mass limit as described above (and a minimum of $M_{*} = 10^{9}\,M_{\odot}$ and $H_{\rm F160W} = 25.5$ at all redshifts), contains 32,722 galaxies; 43 of these are excluded because of catastrophically failed surface brightness profile fits. We then manually verified the spectral energy distribution (SEDs), size measurements, mass, and redshift estimates of all 7,065 objects with flagged GALFIT results ($f = 2$ from van der Wel et al. 2012), small or large sizes ($R_{\rm eff} < 0.6$ kpc; $R_{\rm eff} > 10$ kpc), large stellar masses ($M_{*}/M_{\odot} > 10^{10.8}$), or large differences between photometric and grism redshifts ($\Delta z > 0.15$), as well as all early-type galaxies at redshifts $2 < z < 3$. We removed 1721 (5.3%) after this verification because of errors in the size, redshift, or mass measurements. Hence, we have a final sample of 30,958 galaxies; 21,828 (5189) are at $z > 1$ ($z > 2$).

In Figure 3 we show the rest-frame $(U - V)$-M_{*} distribution, and a clear bimodality is seen, equivalent to the bimodality seen

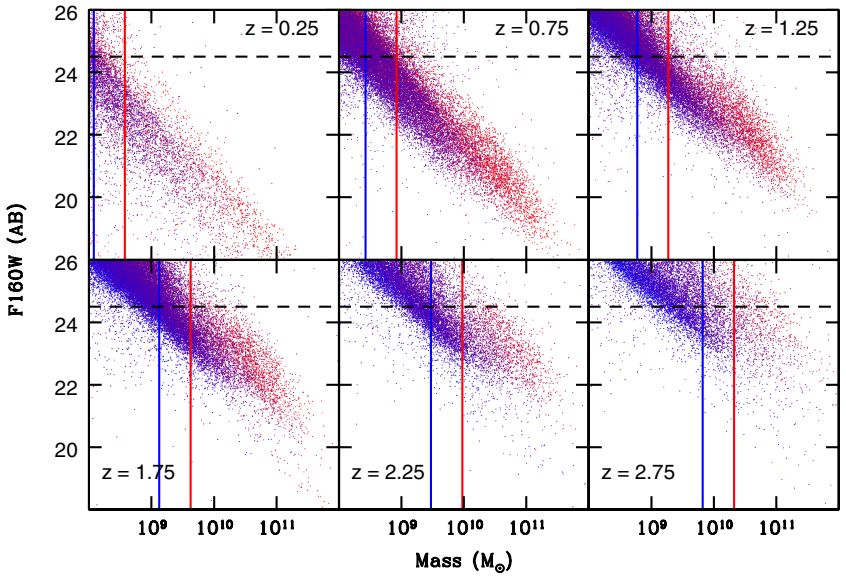

Figure 2. Observed $H_{\rm F160W}$ magnitude vs. stellar mass in six redshift bins. The color coding represents the rest-frame $U-V$ colors, ranging from $U-V=0$ (blue) to $U-V=2$ (red). The horizontal dashed lines indicate the limit ($H_{\rm F160W}=24.5$) down to which we can determine sizes with good fidelity. The vertical lines illustrate the resulting mass completeness limits for blue ($U-V=0.5$) and red ($U-V=2.0$) galaxies, respectively. See Section 2.4 for further details.
(A color version of this figure is available in the online journal.)

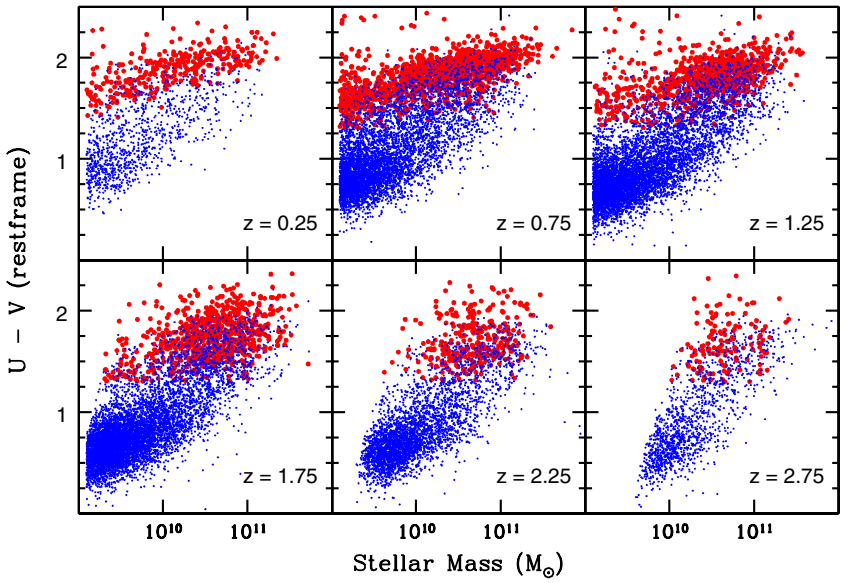

Figure 3. Rest-frame $U-V$ color vs. stellar mass in six redshift bins. Early-type galaxies, defined as illustrated in Figure 1, are shown in red and late types in blue. A clearly defined red sequence is seen up to $z=3$, with an increased prevalence of dusty late-type galaxies toward higher redshifts.
(A color version of this figure is available in the online journal.)

in Figure 1. As is well-known, more massive galaxies are redder and more likely to be quiescent, at least up to $z\sim 2.5$. The most massive galaxies $>10^{11}\,M_{\odot}$ are essentially all red. They are a mix of quiescent and star-forming galaxies; the quiescent galaxies dominate in number at $z<1$, and the star-forming galaxies dominate at $z>2$.

2.5. Size Determinations

Galaxy sizes are measured as described by van der Wel et al. (2012), from mosaics created by the 3D-HST collaboration from public CANDELS F125W and F160W and 3D-HST F140W raw imaging data. With GALFIT we fit single-component Sérsic profiles to the two-dimensional light profiles of all detected objects, making use of custom-made PSF models; the package GALAPAGOS allows for simultaneous fitting of as many neighboring objects as needed, in order to avoid confusion. As the effective radius we use the semi-major axis of the ellipse that contains half of the total flux of the best-fitting Sérsic model. For a full description of the procedure, we refer to van der Wel et al. (2012); the size measurements published and their catalog and the size measurements here are fully consistent.

Color gradients and their evolution affect the size measurements to a degree that greatly exceeds the statistical uncertainties in our sample averages and the size distributions as a function of galaxy mass and redshift. The dynamic range in wavelength for our sample is rather small (from 1.25 μm to 1.6 μm), which does not allow us to systematically probe the effect of color gradients over the large range in redshift. To extend the dynamic

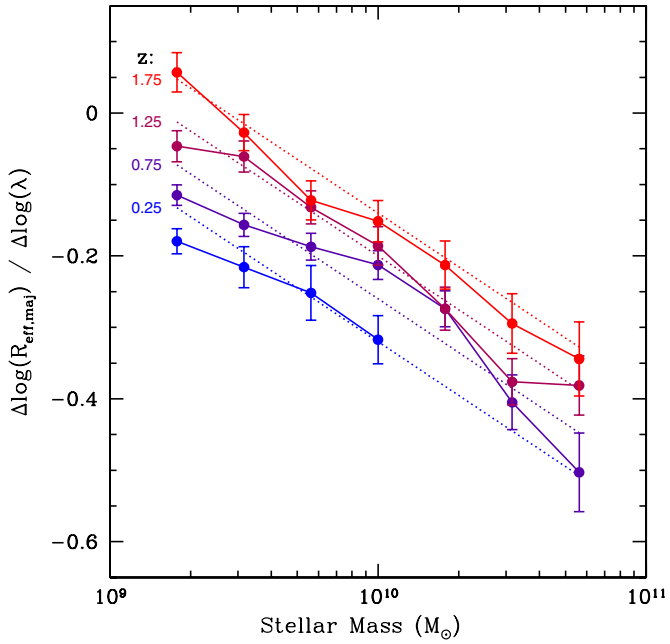

Figure 4. Wavelength dependence of $R_{\rm eff}$ in bins of stellar mass and redshift; the latter is indicated by the color coding. Late-type galaxies, as defined in Figure 1, with robust size measurements from ACS/F814W, WFC3/F125W, and WFC3/F160W imaging are included (see text for details). Generally, sizes are smaller at longer wavelengths, that is, late-type galaxies are bluer in the outer parts. Moreover, this gradient is stronger for more massive galaxies at all redshifts, and the gradient decreases with redshift, at the same rate for all masses. The dotted lines represent the parameterization given in Equation (1) that we use to correct our size measurements of late-type galaxies.

(A color version of this figure is available in the online journal.)

range, we analyze ACS/F814W imaging in the COSMOS field from CANDELS parallel observations. GALAPAGOS is used to obtain galaxy sizes in precisely the same manner for the F814W data as for the WFC3 data.

Using this extension in wavelength, we show in Figure 4 the wavelength dependence of galaxy size for a sample of 777 late-type galaxies. The figure shows $\Delta \log R_{\rm eff}/\Delta \log \lambda$ as a function of galaxy mass and redshift. For galaxies at $z < 1$, the difference between $\log R_{\rm eff}$ from the F814W and F125W size measurements was taken as $\Delta \log R_{\rm eff}$; for $z > 1$ galaxies the difference between $\log R_{\rm eff}$ from the F125W and F160W measurements was taken. The pivot wavelengths of the respective filters are used to compute $\Delta \log \lambda$.

The generally negative values of the quantity $\Delta \log R_{\rm eff}/\Delta \log \lambda$ imply that late-type galaxies are typically smaller at longer wavelengths and thus have negative color gradients (redder centers). The color gradients of $z > 1$ galaxies have been extensively studied before (e.g., Szomoru et al. 2011; Wuyts et al. 2012), and here we merely mention the trends that are relevant for our conversion of the measured $R_{\rm eff}$ to the $R_{\rm eff}$ at a rest-frame wavelength of 5000 Å. Color gradients are strongest for the most massive galaxies at all redshifts and stronger at later cosmic times for galaxies of all masses. The evolution is remarkably smooth, which allows us to parameterize the wavelength dependence of $R_{\rm eff}$ as a simple function of redshift and galaxy stellar mass:

$$\frac{\Delta \log R_{\rm eff}}{\Delta \log \lambda} = -0.35 + 0.12z - 0.25 \log \left(\frac{M_*}{10^{10}\, M_\odot} \right). \quad (1)$$

Kelvin et al. (2012) derive a very similar wavelength dependence of $R_{\rm eff}$, but a direct comparison cannot be made as those authors do not distinguish between galaxies with different masses. Then, $R_{\rm eff}$ at a rest-frame wavelength of 5000 Å is estimated as

$$R_{\rm eff} = R_{\rm eff,F} \left(\frac{1+z}{1+z_p} \right)^{\frac{\Delta \log R_{\rm eff}}{\Delta \log \lambda}}, \quad (2)$$

where F denotes either F125W (for galaxies at $z < 1.5$) or F160W (for galaxies at $z > 1.5$), and z_p is the "pivot redshift" for these respective filters (1.5 for F125W and 2.2 for F160W). Positive color gradients as computed with Equation (1) are set at zero.

A similarly detailed correction for early-type galaxies is currently not feasible as that subsample is much smaller and has much redder colors. For the 122 early-type galaxies in the COSMOS field at redshifts $0 < z < 2$ and with robust size measurements in all three filters, we find an average size gradient of $\Delta \log R_{\rm eff}/\Delta \log \lambda = -0.25$, with no discernible trends with mass and redshift, which is in reasonable agreement with Kelvin et al. (2012) for low-redshift early-type galaxies and Guo et al. (2011) for high-redshift early-type galaxies. Hence, we adopt this value for all early-type galaxies when computing their rest-frame 5000Å sizes with Equation (2).

This rather convoluted procedure has a small but significant effect on the size measurements, with implications for the rate of size evolution. In the redshift range $1 < z < 2$, the size corrections are always smaller than 0.05 dex because the observed wavelength is always close to the desired rest-frame wavelength; at $z < 1$ the correction can increase up to 0.15 dex, but there the color gradient is well constrained (see Figure 4) for all galaxy masses.

3. EVOLUTION OF THE SIZE–MASS DISTRIBUTION AT $0 < z < 3$

The size–mass distributions for early- and late-type galaxies as a function of redshift are shown in Figure 5. The first basic observation is that a well-defined size–mass relation exists at all redshifts $0 < z < 3$ for both populations. With increasing redshift, the two classes have increasingly different size–mass relations, mostly as a result of strongly decreasing $R_{\rm eff}$ for early types. In addition, at all redshifts the slope of the relation is steeper for early types than for late types. At all stellar masses $\lesssim 10^{11}\, M_\odot$ early-type galaxies are, on average, smaller than late-type galaxies, but at very high stellar masses ($>2 \times 10^{11}\, M_\odot$) the two populations have similar sizes at all redshifts, as far as the small samples allow for such a comparison.

However, the relation for early-type galaxies flattens out below $M_* = 2 \times 10^{10} M_\odot$, at least up to $z = 1.5$, beyond which our sample is incomplete at these low masses. This implies that the peak in surface mass density at $\sim 4 \times 10^{10}\, M_\odot$ seen in the present-day universe also existed at larger look-back times, at least up to $z \sim 2$.

In Section 3.1 we will first provide an analytical description of the size–mass relation, which allows us to take cross-contamination between the two types and outliers into account. In the remainder of this section we will provide various direct measurements such as median sizes and percentile distributions as a function of mass and redshift and describe trends that are not captured by our analytical description, such as deviations from a single power law and skewness of the size distribution.

3.1. Analytical Description

The basic characteristics of the galaxy size distribution are given by the slope, intercept, and (intrinsic) scatter of size as

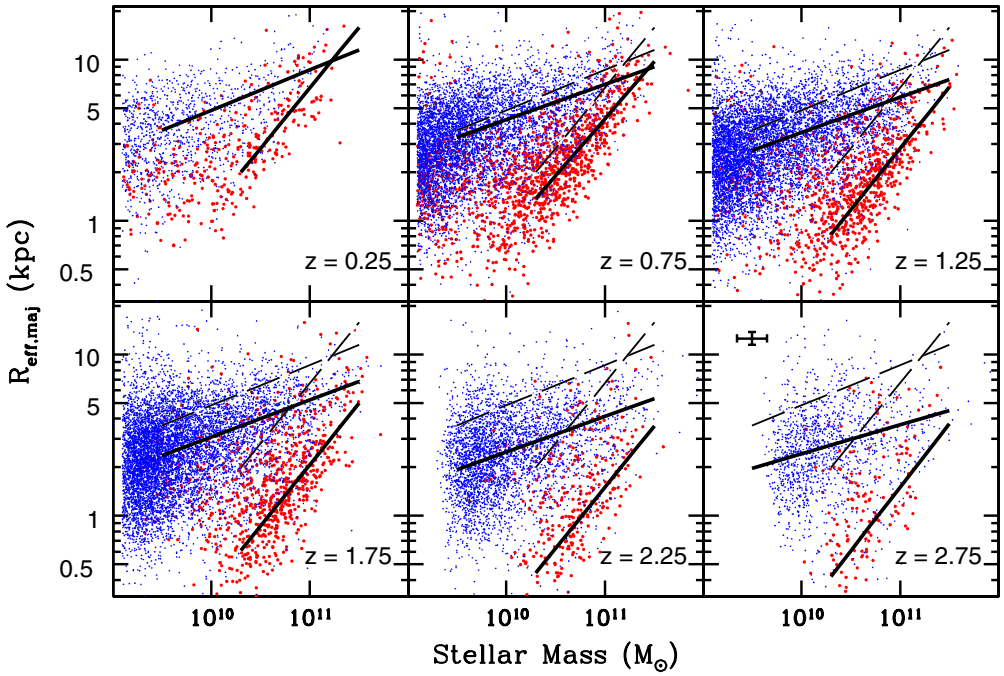

Figure 5. Size–stellar mass distribution of late- and early-type galaxies (same symbols as in Figure 2). A typical 1σ error bar for individual objects in the higher-redshift bins is shown in the bottom right panel. The lines indicate model fits to the early- and late-type galaxies as described in Section 3.1. The dashed lines, which are identical in each panel, represent the model fits to the galaxies at redshifts $0 < z < 0.5$. The solid lines represent fits to the higher-redshift samples. The mass ranges used in the fits are indicated by the extent of the lines in the horizontal direction. Strong evolution in the intercept of the size–mass relation is seen for early-type galaxies, and moderate evolution is seen for the late-type galaxies (also see Figure 6. There is no significant evidence for evolution in the slope (also see Figure 6). The parameters of the fits shown here are given in Table 1.

(A color version of this figure is available in the online journal.)

a function of mass. We parameterize this following Shen et al. (2003) and assume a log-normal distribution $N(\log r, \sigma_{\log r})$, where $\log r$ is the mean and $\sigma_{\log r}$ is the dispersion. Furthermore, r is taken to be a function of galaxy mass:

$$r(m_*)/\mathrm{kpc} = \mathrm{A} \cdot \mathrm{m}_*^{\alpha}, \quad (3)$$

where $m_* \equiv M_*/7 \times 10^{10}\,M_\odot$. As we will describe in Section 3.3, it is reasonable to assume that $\sigma_{\log r}$ is independent of mass.

The model distribution $N(\log r(m_*), \sigma_{\log r})$ prescribes the probability distribution for observing $R_{\rm eff}$ for a galaxy with mass m_*. If the measured $R_{\rm eff}$ has a Gaussian, 1-σ uncertainty of $\delta \log R_{\rm eff}$, then the probability for this observation is the inner product of two Gaussians:

$$P = \langle N(\log R_{\rm eff}, \delta \log R_{\rm eff}), N(\log r(m_*), \sigma_{\log r})\rangle. \quad (4)$$

Thus, we compute for each galaxy the probabilities $P_{\rm ET}$ and $P_{\rm LT}$ for the respective size–mass distribution models for the early-type and late-type populations. Incompleteness terms should formally be included in these probabilities (as described by, e.g., Huang et al. 2013), but because of our conservative sample selection (see Section 2.4) we are not biased against faint, large objects.

The uncertainty in size, $\delta \log R_{\rm eff}$, is computed as outlined by van der Wel et al. (2012). A random uncertainty of 0.15 dex in m_* is included in our analysis by treating it as an additional source of uncertainty in $R_{\rm eff}$: for a size–mass relation with a given slope, an offset in m_* translates into an offset in $R_{\rm eff}$. Hence, the calculation of P stays one-dimensional. The fiducial slopes we use to convert $\delta \log R_{\rm eff}$ into δm_* are $\alpha = 0.7$ for early-type galaxies and $\alpha = 0.2$ for late-type galaxies.

We also take into account the misclassification of early- and late-type galaxies. Despite the bimodal distribution in the color–color diagram (Section 2.4; Figure 1), there are galaxies in the region between the star-forming and quiescent sequences, making their classification rather arbitrary and causing cross-contamination of the two classes (also see Holden et al. 2012). Motivated by this work, we take this misclassification probability to be 10%. We will comment on the effects of varying this parameter below, when we describe the fitting results.

The misclassification probability precisely corresponds to the early- and late-type contamination fractions in a sample in cases where the two subsamples have an equal number of galaxies. The actual contamination fraction scales with the early- and late-type fractions, which depend on galaxy mass and redshift. The evolution of the stellar mass function for the two types is described by Muzzin et al. (2013), which we use here to compute this ratio. We also allow for 1% of outliers: these are objects that are not part of the galaxy population, for example, catastrophic redshift estimates or misclassified stars. Finally, in order to avoid being dominated by the large number of low-mass galaxies, we also assign a weight to each galaxy that is inversely proportional to the number density. This ensures that each mass range carries equal weight in the fit. The number density is taken from the Muzzin et al. (2013) mass functions.

Then, we compute the total likelihood for a set of six model parameters (intercept A, slope α, and intrinsic scatter $\sigma_{\log R_{\rm eff}}$, each for both types of galaxies):

$$\mathcal{L}_{\rm ET} = \sum \ln[W \cdot ((1-C) \cdot P_{\rm ET} + C \cdot P_{\rm LT} + 0.01)] \quad (5)$$

for early-type galaxies, and

$$\mathcal{L}_{\rm LT} = \sum \ln[W \cdot ((1-C) \cdot P_{\rm LT} + C \cdot P_{\rm ET} + 0.01)] \quad (6)$$

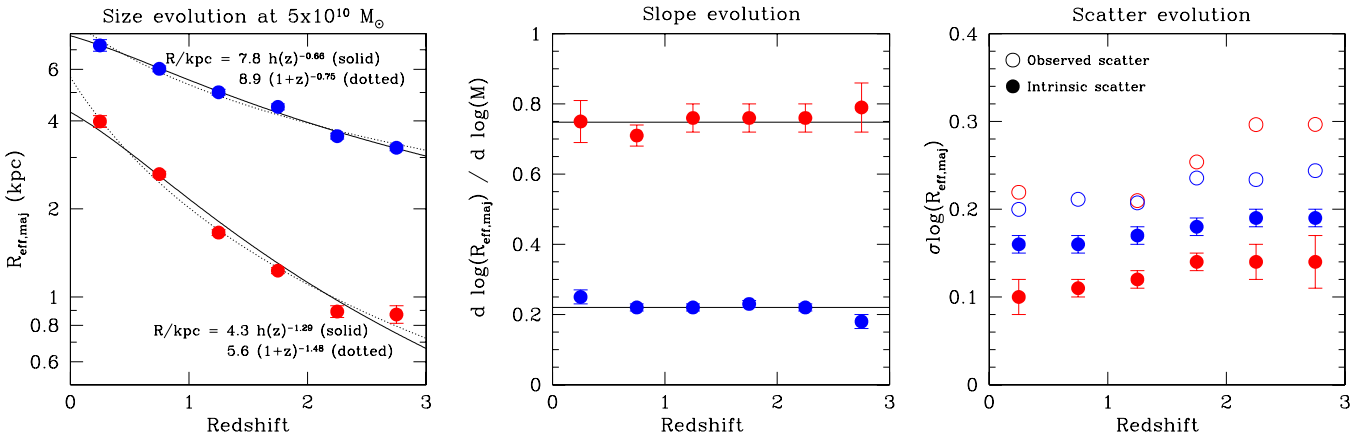

Figure 6. Parameterized redshift evolution of the size–mass relation, from the power law model fits shown in Figure 5. The left-hand panel shows the evolution of the intercept, or the size evolution at fixed stellar mass of $5 \times 10^{10} M_{\odot}$. Strong evolution is seen for high-mass early-type galaxies, and moderate evolution is seen for low-mass early types and for late-type galaxies. The middle and right-hand panels show the evolution of the slope and intrinsic (model) scatter of the size–mass relation, either with little or no evidence for changes with redshift. The open symbols represent the observed scatter: these measurements do not take measurement uncertainties and contamination into account. The fitting parameters shown in this figure are given in Table 1.

(A color version of this figure is available in the online journal.)

Table 1
Results from the Parameterized Fits to the Size–Mass Distribution of the form $R_{\rm eff}/{\rm kpc} = A(M_*/5 \times 10^{10}\, M_{\odot})^{\alpha}$, as Described in Section 3.1 and Shown in Figures 5 and 6

	Early-type Galaxies			Late-type Galaxies		
z	$\log(A)$	α	$\sigma\log(R_{\rm eff})$	log A	α	$\sigma\log(R_{\rm eff})$
0.25	0.60 ± 0.02	0.75 ± 0.06	0.10 ± 0.02	0.86 ± 0.02	0.25 ± 0.02	0.16 ± 0.01
0.75	0.42 ± 0.01	0.71 ± 0.03	0.11 ± 0.01	0.78 ± 0.01	0.22 ± 0.01	0.16 ± 0.01
1.25	0.22 ± 0.01	0.76 ± 0.04	0.12 ± 0.01	0.70 ± 0.01	0.22 ± 0.01	0.17 ± 0.01
1.75	0.09 ± 0.01	0.76 ± 0.04	0.14 ± 0.01	0.65 ± 0.01	0.23 ± 0.01	0.18 ± 0.01
2.25	-0.05 ± 0.02	0.76 ± 0.04	0.14 ± 0.02	0.55 ± 0.01	0.22 ± 0.01	0.19 ± 0.01
2.75	-0.06 ± 0.03	0.79 ± 0.07	0.14 ± 0.03	0.51 ± 0.01	0.18 ± 0.02	0.19 ± 0.01

Note. $\sigma(\log R_{\rm eff})$ is the scatter in $R_{\rm eff}$ in logarithmic units.

for late-type galaxies, where W is the weight and C is the contamination fraction, both of which are a function of redshift and mass. The best-fitting parameters are identified by finding the model with the maximum total likelihood, $\mathcal{L} = \mathcal{L}_{\rm ET} + \mathcal{L}_{\rm LT}$.

For the late types, we fit all galaxies with $M_* > 3 \times 10^9 M_{\odot}$; this limit provides a good dynamic range of two orders of magnitude in mass and exceeds the mass limit of our sample up to $z = 2.5$ (Figure 2). For the early types, we fit all galaxies with $M_* > 2 \times 10^{10} M_{\odot}$, so that we avoid the clearly flatter part of the size–mass distribution at lower masses (see Section 3.2). This cutoff exceeds the mass limit of our sample up to $z = 3$.

The black lines in Figure 5 indicate the fitting results, and the evolution of the individual model parameters (intercept, slope, and scatter) are shown in Figure 6. The fitting results are also given in Table 1. The intercept of the best-fitting size mass model distributions evolves significantly with redshift and particularly rapidly for the early types.

Usually, the evolution of the intercept is parameterized as a function of $(1+z)$. While this is intuitively appealing because of our familiarity with the cosmological scale factor, this is perhaps not the physically most meaningful approach. Galaxy sizes, in particular disk scale lengths, are more directly related to the properties of their dark matter halos than to the cosmological scale factor. Halo properties such as virial mass and radius follow the evolving expansion rate—the Hubble parameter $H(z)$—instead of the cosmological scale factor. For a matter-dominated universe, $H(z)$ and $(1 + z)$ evolve at a similar pace, but as a result of the increased importance at late times of Λ for the dynamical evolution of the universe, $H(z)$ evolves much slower in proportion to $(1 + z)$ at late times than at early times. For example, at $z \sim 0$ we have $H(z) \propto (1+z)^{0.4}$, while at $z \sim 2$ this is $H(z) \propto (1 + z)^{1.4}$.

For this reason it is reasonable to parameterize size evolution as a function of $H(z)$ in addition to $(1 + z)$. The solid lines in the left-hand panel of Figure 6 represent the evolution as a function of $H(z)$, while the dashed lines represent the evolution as a function of $(1 + z)$. These results are also given in Table 1. The $H(z)^{\beta_H}$ parameterization is marginally preferred by the data over the $(1 + z)^{\beta_z}$ parameterization, as is more clearly illustrated in Figure 7, where we show the residuals. In addition to the statistical limitations, we note that these residuals are of the same magnitude as the systematic uncertainties in the size measurements and color gradient corrections (Section 2.5). A more thorough comparison with size evolution of larger samples at $z < 1$ with size measurements at visual wavelengths would improve these constraints.

Newman et al. (2012) first demonstrated the lack of strong evolution in the slope of the size–mass relation for massive ($>2 \times 10^{10}\, M_{\odot}$) early-type galaxies. Here we confirm that result (middle panel, Figure 6) and find a slope of $R_{\rm eff} \propto M^{0.75}$ at all redshifts. This slope is somewhat steeper than measured by Shen et al. (2003) for present-day early-type galaxies. Differences in sample selection (star-formation activity versus concentration) and methods ($R_{\rm eff}$ from Sérsic profile fits versus Petrosian

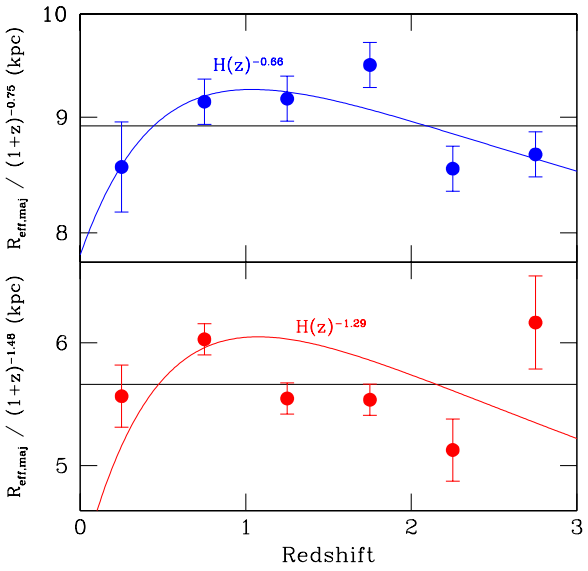

Figure 7. Evolution-corrected average sizes at $M_* = 5 \times 10^{10}\ M_\odot$ for late-type galaxies (top panel, in blue) and early-type galaxies (bottom panel, in red). The values shown here are the values shown in the left-hand panel of Figure 6, divided by $(1+z)^{\beta_z}$ as indicated on the y-axis. The residuals from the best-fitting $(1+z)^{\beta_z}$ law indicate that parameterizing the evolution as a function of the Hubble parameter ($R_{\rm eff} \propto h(z)^{\beta_H}$) may provide a more accurate description of the late-type galaxies. See Section 3.2 for further discussion.

(A color version of this figure is available in the online journal.)

half-light radii) may explain this difference. For the first time we extend the analysis to late-type galaxies: the slope is much flatter than the slope for early types ($R_{\rm eff} \propto M^{0.22}$), with little or no change with redshift. This slope is intermediate to the slope found by Shen et al. (2003) for low- and high-mass galaxies. Our sample contains too few high-mass late-type galaxies to perform a robust double-component power law fit, as done by Shen et al. (2003), but in Section 3.2 we will show evidence for the steepening of the relation for massive late-type galaxies out to $z = 1$.

Finally, we present the first measurement of the intrinsic scatter in size beyond the local universe (right-hand panel of Figure 6). We find no strong evolution for either late types or early types, and we find that the scatter for the early-type population is always somewhat smaller (0.1–0.15 dex) than for the late-type population (0.16–0.19 dex). These numbers agree well with the intrinsic scatter measured by Shen et al. (2003) for present-day galaxies: 0.13 dex for early-type galaxies and 0.20 dex for late-type galaxies. We note that the effects of measurement uncertainties were not included by Shen et al. (2003).

For comparison, we show the observed scatter at each redshift, calculated as the standard deviation in $R_{\rm eff}$ after subtracting the best-fitting size–mass relation. The values for early-type galaxies are in the range of 0.2–0.3 dex, in good agreement with the values found by (Newman et al. 2012) over the same redshift range. In particular, the strongly increased observed scatter in size for the early-type galaxies at $z > 2$ is largely attributed to significant contamination by misclassified late-type galaxies. We have assumed a misclassification probability of 10% (resulting in an assumed misclassified fraction of $C = 0.10$ in the case of an equal number of early- and late-type galaxies—see above), but although this value is empirically motivated, it is not known with great precision. If we decrease (increase) the misclassification probability to 5% (20%), then the recovered intrinsic scatter for the $z = 2.0$–2.5 early-type galaxy sample, for example, increases (decreases) to 0.18 (0.11).

At this point we should also comment on the effect of changing the value for the assumed random uncertainty in stellar mass (here 0.15 dex). Decreasing its value has no measurable effect, while increasing it to 0.30 dex decreases the recovered value for the intrinsic scatter further, to 0.05 dex for the $z = 2.0$–2.5 early-type galaxy sample. In this sense, the derived values for the intrinsic scatter are upper limits.

While our particular choices in modeling the uncertainties affect the results with (marginal) significance, they do not affect our general conclusions that the intrinsic size scatter (1) is $\lesssim$0.20 dex for both types of galaxies and (2) does not strongly evolve with redshift. However, the conclusion that the scatter for early-type galaxies is smaller than for late-type galaxies at all redshifts—as is seen for present-day galaxies—should at this stage be regarded as tentative.

Finally, we note that changes in the misclassification probability or uncertainty in stellar mass do not significantly affect the recovered values of the other model parameters (zero point and slope).

3.2. Evolution of Median Sizes

In this section we offer a complementary description of the evolution of the size–mass relation. In Figure 8 we show the median sizes as a function of mass and redshift, along with the 68th percentile width of the size distribution. The values are listed in Table 2. Up to $z \sim 1.5$ the relation for late types steepens and tightens at the high-mass end. Shen et al. (2003) modeled the steepening by assuming a two-component power law, but we sample an insufficiently large volume and sample size at $>10^{11}\ M_\odot$ to include this in our analytical description presented above (Section 3.1). The flattening of the size–mass relation for low-mass early types is also clearly seen. Inspection of the SEDs of individual galaxies confirms that these are truly quiescent galaxies, with strong 4000 Å breaks. As we showed in Section 3.1, the large apparent increase in the scatter for high-redshift early types can be partially attributed to contaminants and outliers.

We provide complementary sets of median size and scatter measurements in the Appendix. These include the commonly used circularized radii: $R_{\rm eff,circ} = R_{\rm eff}\sqrt{b/a}$, where b/a is the projected axis ratio. In addition, we provide the measurements for the combined late + early-type galaxy sample and the measurements in bins of rest-frame V-band luminosity.

Figure 9 shows the median size evolution for galaxies in different mass bins. We parameterize this evolution both as a function of $H(z)$ and of $(1+z)$—see Section 3.1. The results are shown as solid and dotted lines, respectively, in Figure 9 and are also given in Table 2.

Ideally, an immediate comparison with the size–mass distribution of nearby galaxies provides a strong constraint on the evolution. However, such comparisons are fraught with systematic uncertainties. The aim here is merely to show that our observations from CANDELS and 3D-HST are consistent with the size–mass relation for nearby galaxies as measured from the SDSS (Shen et al. 2003), who provided the standard reference for this purpose.

In order to account for possible systematic differences we compare the size measurements from Shen et al. (2003) with those from Guo et al. (2009) on an object-by-object basis. The reason for using the Guo et al. (2009) measurements as a baseline is that they are based on the same technique—GALAPAGOS

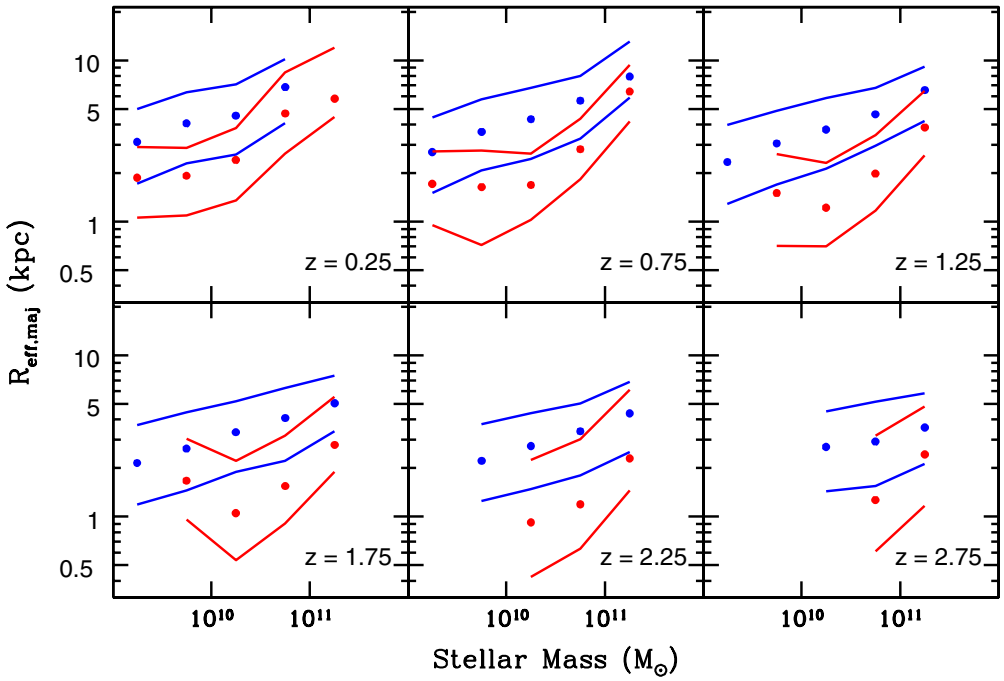

Figure 8. Median (points) and 16th and 84th percentiles (lines) of the size–stellar mass distributions shown in Figure 5. The scatter in $R_{\rm eff}$ does not strongly depend on galaxy mass. Deviations from the power law form of the size–mass relation are clear for massive late-type galaxies and for low-mass early-type galaxies. Note that here we do not account for contamination (misclassified early- and late-type galaxies).

(A color version of this figure is available in the online journal.)

Table 2
Logarithmic Size Distribution (16%–84% Range) as a Function of Galaxy Mass and Redshift

		Early-type Galaxies					Late-type Galaxies				
z		$M_* = 10^{9.25}$	9.75	10.25	10.75	11.25	9.25	9.75	10.25	10.75	11.25
	16%	0.03 ± 0.06	0.04 ± 0.03	0.13 ± 0.03	0.42 ± 0.02	0.65 ± 0.05	0.24 ± 0.01	0.36 ± 0.02	0.42 ± 0.02	0.61 ± 0.03	...
0.25	50%	0.27 ± 0.02	0.28 ± 0.02	0.38 ± 0.03	0.67 ± 0.02	0.76 ± 0.09	0.49 ± 0.01	0.61 ± 0.02	0.66 ± 0.03	0.83 ± 0.03	...
	84%	0.46 ± 0.03	0.46 ± 0.04	0.58 ± 0.04	0.92 ± 0.05	1.08 ± 0.08	0.70 ± 0.01	0.80 ± 0.01	0.85 ± 0.02	1.01 ± 0.04	...
	16%	-0.02 ± 0.03	-0.14 ± 0.02	0.02 ± 0.02	0.26 ± 0.01	0.62 ± 0.02	0.18 ± 0.01	0.32 ± 0.01	0.39 ± 0.01	0.51 ± 0.02	0.77 ± 0.02
0.75	50%	0.23 ± 0.01	0.21 ± 0.02	0.23 ± 0.01	0.45 ± 0.01	0.81 ± 0.02	0.43 ± 0.01	0.56 ± 0.01	0.64 ± 0.01	0.75 ± 0.01	0.90 ± 0.04
	84%	0.43 ± 0.02	0.44 ± 0.02	0.42 ± 0.02	0.64 ± 0.02	0.97 ± 0.02	0.65 ± 0.01	0.76 ± 0.01	0.83 ± 0.01	0.90 ± 0.01	1.12 ± 0.03
	16%	...	-0.15 ± 0.03	-0.15 ± 0.02	0.07 ± 0.01	0.41 ± 0.02	0.11 ± 0.01	0.23 ± 0.01	0.33 ± 0.01	0.47 ± 0.01	0.62 ± 0.03
1.25	50%	...	0.18 ± 0.03	0.09 ± 0.02	0.30 ± 0.01	0.58 ± 0.03	0.37 ± 0.01	0.48 ± 0.01	0.57 ± 0.01	0.67 ± 0.01	0.82 ± 0.03
	84%	...	0.42 ± 0.04	0.36 ± 0.03	0.54 ± 0.03	0.81 ± 0.03	0.60 ± 0.01	0.69 ± 0.00	0.77 ± 0.01	0.83 ± 0.01	0.96 ± 0.02
	16%	...	-0.02 ± 0.06	-0.27 ± 0.02	-0.04 ± 0.02	0.28 ± 0.02	0.07 ± 0.01	0.16 ± 0.01	0.28 ± 0.01	0.35 ± 0.02	0.53 ± 0.04
1.75	50%	...	0.22 ± 0.03	0.02 ± 0.03	0.19 ± 0.02	0.45 ± 0.02	0.33 ± 0.01	0.42 ± 0.01	0.52 ± 0.01	0.61 ± 0.01	0.70 ± 0.02
	84%	...	0.48 ± 0.06	0.35 ± 0.03	0.50 ± 0.03	0.74 ± 0.04	0.57 ± 0.01	0.65 ± 0.01	0.72 ± 0.01	0.80 ± 0.01	0.87 ± 0.02
	16%	...	...	-0.37 ± 0.08	-0.20 ± 0.02	0.16 ± 0.03	...	0.10 ± 0.01	0.17 ± 0.02	0.26 ± 0.03	0.40 ± 0.02
2.25	50%	...	...	-0.04 ± 0.07	0.08 ± 0.03	0.36 ± 0.05	...	0.35 ± 0.01	0.44 ± 0.01	0.53 ± 0.01	0.64 ± 0.02
	84%	...	...	0.36 ± 0.03	0.54 ± 0.04	0.55 ± 0.07	...	0.57 ± 0.01	0.64 ± 0.01	0.70 ± 0.01	0.84 ± 0.02
	16%	...	...	...	-0.22 ± 0.05	0.07 ± 0.07	...	...	0.16 ± 0.02	0.19 ± 0.06	0.33 ± 0.04
2.75	50%	...	...	...	0.10 ± 0.03	0.39 ± 0.08	...	...	0.43 ± 0.01	0.47 ± 0.01	0.55 ± 0.02
	84%	...	...	...	0.50 ± 0.10	0.68 ± 0.10	...	...	0.65 ± 0.02	0.71 ± 0.02	0.76 ± 0.04
	$\log B_z$	...	0.29 ± 0.01	0.47 ± 0.02	0.75 ± 0.04	1.05 ± 0.09	0.54 ± 0.01	0.69 ± 0.01	0.74 ± 0.03	0.90 ± 0.05	1.05 ± 0.08
	$\log \beta_z$	...	-0.22 ± 0.02	-1.01 ± 0.06	-1.24 ± 0.08	-1.32 ± 0.21	-0.48 ± 0.03	-0.63 ± 0.02	-0.52 ± 0.08	-0.72 ± 0.09	-0.80 ± 0.18
	$\log B_H$	...	0.27 ± 0.01	0.42 ± 0.02	0.68 ± 0.03	0.97 ± 0.06	0.52 ± 0.01	0.65 ± 0.01	0.71 ± 0.03	0.86 ± 0.04	1.01 ± 0.06
	$\log \beta_H$	...	-0.19 ± 0.02	-0.97 ± 0.05	-1.13 ± 0.06	-1.29 ± 0.16	-0.52 ± 0.02	-0.58 ± 0.02	-0.49 ± 0.07	-0.65 ± 0.09	-0.76 ± 0.13

Notes. The masses in the header and the redshifts in the first column are the centers of 0.5-wide bins. Redshift dependence in the form $R_{\rm eff}/{\rm kpc} = B_z(1+z)^{\beta_z}$ and $R_{\rm eff}/{\rm kpc} = B_H(H(z)/H_0)^{\beta_H}$ are also given.

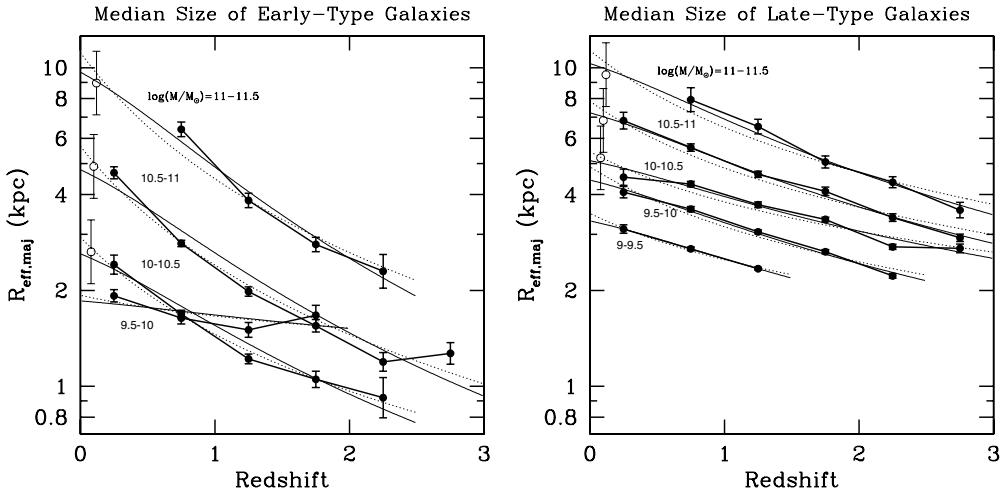

Figure 9. Median size as a function of stellar mass and redshift for early-type galaxies (left) and late-type galaxies (right). SDSS data points based on (Guo et al. 2009) are shown as open points. Fits to the median sizes of the form $R_{\rm eff}/{\rm kpc} = {\rm B}_z(1+z)^{\beta_z}$ and $B_H(H(z)/H_0)^{\beta_H}$ are shown by dotted and solid lines, respectively. The evolution of the early-type galaxies is independent of mass at $M_* > 2 \times 10^{10}\,M_\odot$: massive galaxies evolve fast and have a steep size–mass relation at all redshifts, while the relation flattens out at lower masses ($\lesssim 10^{10} M_\odot$) and evolves less rapidly. The evolution of the late-type galaxies is overall slower and does not depend strongly on mass. The low-mass early-type galaxies evolve at the roughly the same pace as the late-type galaxies. The median sizes and fitting results are given in Table 2.

from Barden et al. (2012)—as used in this paper. We shift the analytical descriptions of the size–mass relations from Shen et al. (2003) according to the measured, systematic offset between Shen et al. (2003) and Guo et al. (2009). This amounts to a 0.1 dex shift to larger $R_{\rm eff}$ than Shen et al. (2003).[18] In order to be conservative, we also adopt 0.1 dex as the systematic uncertainty. We show the inferred sizes for local galaxies in Figure 9. The median size evolution traced out by the 3D-HST/CANDELS data predicts $z \sim 0$ sizes that are consistent with our adjusted Shen et al. (2003) median sizes.

The picture provided by median size distributions is consistent with our analytical description (Section 3.1), with fast evolution for the (massive) early types and moderate evolution for the late types. In addition, we see that the flattening of the relation for low-mass early types coincides with slower evolution. Interestingly, low-mass early-type galaxies evolve at a similar same rate as late types of the same mass. For the late types we see a mild dependence on mass: the more massive late types evolve slightly faster than the less massive late types. For further discussion, see Section 5.

3.3. Skewness in the $R_{\rm eff}$ Distribution of Late-type Galaxies

The 16- and 84-percentile range for late-type galaxies is not precisely centered on the median size (Figure 8 and Table 2), implying a skewness in the size distribution. To examine this further, we show size distribution histograms for a set of mass and redshift bins in Figure 10. The asymmetric size distribution for late-type galaxies is due to a tail of small galaxies. The small sizes are not due to pointlike contributions from active galactic nucleus (AGN): the 1–10 μm photometry of these objects does not show the power law SEDs that are characteristic for unobscured AGN.

As a result of this skewness, there is substantial overlap between the size distributions of early types and late types and no clear bimodality, despite large differences in the average sizes. Figure 11 shows more clearly than Figure 10 that the size distributions of the two types overlap at all redshifts, up to $z \sim 3$.

Figure 10 also shows tails of large early-type galaxies. However, this can likely be attributed to misclassification: their number is always an order magnitude smaller than the number of late-type galaxies with similar sizes, consistent with the assumed misclassification probability in our analysis in Section 3.1. We note that the tail of small late-type galaxies is not consistent with the expected number of misclassificated objects: its prominence appears to be unrelated to the early-type population.

As an illustration that the size distribution for both early- and late-type galaxies evolve smoothly and regularly, we fit Hermite–Gaussian functions to the histograms shown in Figure 10. This provides a reasonable description of all redshift and mass bins.

For a discussion of the implications of these results in the context of previous results, we refer to Sections 4.2 and 5.2.

4. COMPARISON WITH PREVIOUS RESULTS

4.1. Late-type Galaxies

The results for size evolution of late-type galaxies shown in Figures 6 and 9 are consistent with most other recent measurements that focus on the $z = 1$–2 redshift range (e.g., Franx et al. 2008; Buitrago et al. 2008). Williams et al. (2010) found somewhat faster evolution for late types (and slower evolution for early types), but a direct comparison with their Figure 4 reveals that their size measurements and our measurements are in fact fully consistent over the redshift range $0.5 < z < 1.5$. The difference in the quoted pace of evolution is likely the result of the increased dynamic range in redshift probed here, in addition to the use of a low-redshift comparison sample from the SDSS (see Section 3.2).

Thus, like previous studies focusing on the $z = 1$–2 redshift regime, we find that the pace of evolution for late-type galaxies is intermediate to the slow evolution of disk galaxies at $z < 1$ (Lilly et al. 1998; Ravindranath et al. 2004; Barden et al. 2005) and the fast evolution of UV-selected galaxies at $z > 2$ (Giavalisco et al. 1996; Ferguson et al. 2004; Oesch et al. 2010; Mosleh

[18] Note that we use major axis $R_{\rm eff}$ in this paper, as opposed to Shen et al. (2003), who use circularized radii

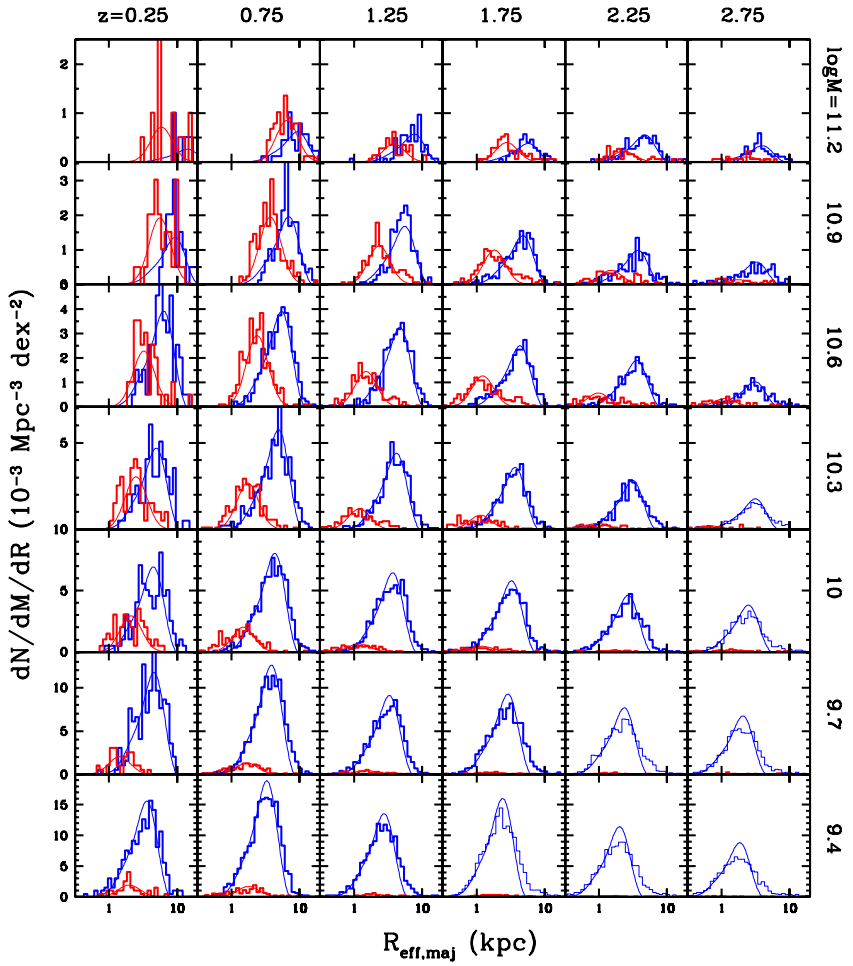

Figure 10. Size distribution histograms for early- and late-type galaxies as a function of stellar mass (as labeled on the right-hand side) and redshift (as labeled at the top). The number of galaxies is given in units of comoving volume to illustrate the growth of the population over time. The early-type size distributions are fit with Gaussians with a fixed dispersion of 0.16 dex. The late-type size distributions are fit with skewed Gaussians with a fixed dispersion of 0.18 dex and skewness $h_3 = -0.15$. The panels with thin lines show samples that are below our mass limit.

(A color version of this figure is available in the online journal.)

et al. 2012). Our data set allows us to bridge these regimes and probe the origin of this difference.

In Figure 12 we show the size evolution of galaxies with stellar mass $M_* \sim 10^{10}\,M_\odot$ from the present day up to $z \sim 6$. Here we have relaxed our magnitude limit to $H_{\rm F160W} = 26$, which is still within the completeness limit of the CANDELS imaging as can be seen in Figure 2. Size measurements of individual galaxies are no longer reliable at $H_{\rm F160W} = 26$, but the sample average is still robust to within 15% (van der Wel et al. 2012). Using a color cut of $U - V < 1$, we can probe a population akin to LBGs out to $z \sim 6$. The median size evolves quickly with redshift, $R_{\rm eff} \propto (1+z)^{-1.1}$, consistent with recent measurements by Oesch et al. (2010) and Mosleh et al. (2012).

Once we include all late-type galaxies, regardless of color, the evolution matches that of the $U - V < 1$ galaxies at $z \gtrsim 2$. This is simply because essentially all galaxies are blue: the color-blind sample is not biased against galaxies with $U - V > 1$ up to $z = 3$–3.5. At lower redshift, red star-forming galaxies appear, which are smaller in size than their blue counterparts and slow down the average size evolution. At $z < 1$, UV-bright galaxies are rare and the evolution is dominated by redder galaxies, which evolve in size more slowly in agreement with the results from, for example, Barden et al. (2005).

As we argued in Section 3.2, galaxy sizes may be better parameterized as a function of $H(z)$ than as a function of $(1+z)$. While the former naturally implies slower evolution at late times than the latter (see the red dotted line in Figure 12), not all trends are captured by using the $H(z)$ parameterization: (1) the evolution of all late types slows down more rapidly than can be explained by the difference between the two parameterizations, and (2) the UV-bright sample shows little evidence for slowed evolution at $z \lesssim 1$.

We conclude that the diverging pace of evolution seen at $z < 1$ and $z > 3$ as reported in the literature is partly due to sample selection effects and partly due to the different evolution of red and blue late-type galaxies.

4.2. Early-type Galaxies

As we discussed in the Introduction, there is broad agreement that the average sizes of $\sim L^*$ early-type galaxies, as measured at a fixed stellar mass, were smaller at high redshift. Moderate deviations in the pace of evolution can be attributed to sample selection, measurement, and/or fitting techniques. For example, as we mentioned above, whereas the size measurements reported by Williams et al. (2010) are consistent with our size measurements, the reported pace of evolution is somewhat different: $(1+z)^{-1}$ from Williams et al. (2010) and $(1+z)^{-1.3}$ from

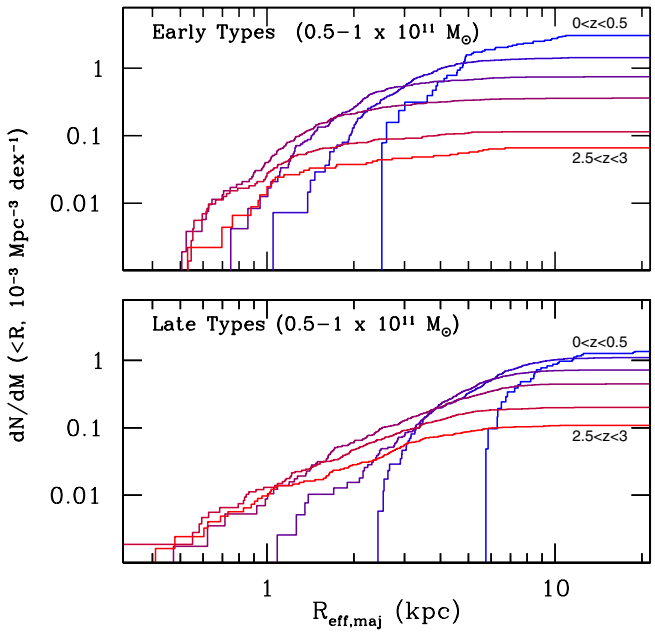

Figure 11. Cumulative size distributions of $\sim L^*$ early-type galaxies (top) and $\sim L^*$ late-type galaxies (bottom) as a function of redshift. While the number density of both early- and late-type galaxies increases over time, the number density of small galaxies declines, implying that the observed evolution in the mean size is not (solely) driven by the addition of larger galaxies. Individual galaxies must evolve in size.

(A color version of this figure is available in the online journal.)

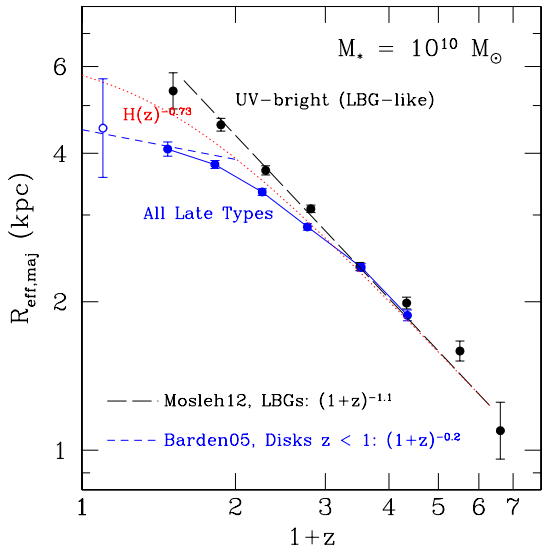

Figure 12. Size evolution of galaxies in a narrow (0.3 dex) mass bin around $10^{10}\,M_\odot$. The black points represent UV-bright galaxies (with $U-V<1$ in the rest-frame), selecting a sample akin to LBGs at high redshift. Their size evolution is fast, consistent with the size evolution of UV-selected samples up to $z=7$ as recently determined by Mosleh et al. (2012)—also see Oesch et al. (2010). The blue points represent late-type galaxies as defined in this paper (see Figure 1), that is, all star-forming galaxies. The size evolution of those is slower at low redshift, consistent with previous measurements at $z<1$ (here, Barden et al. 2005).

(A color version of this figure is available in the online journal.)

Section 3.2 in this paper. This is the result of the difference in spanned redshift range and the different use of present-day comparison samples. While these differences are large enough to be interesting, there is a reasonable consensus that the average size for the population of early-type galaxies evolves rapidly. In particular, the first *HST*/NICMOS-based studies produced an

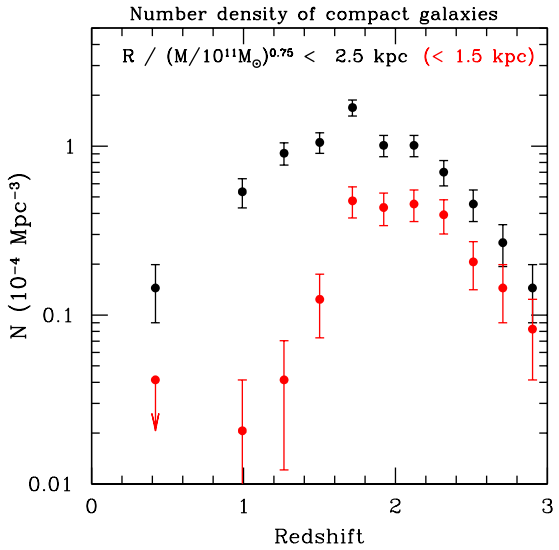

Figure 13. Number density evolution of compact early-type galaxies. In each redshift bin (with equal comoving volume), we include early-type galaxies with mass $M_*>5\times10^{10}\,M_\odot$ and size $R_{\rm eff}({\rm kpc})<(M_*/5\times10^{10}\,M_\odot)^{0.7}$. That is, the slope of the size–mass relation is taken into account: for $M_*=5\times10^{10}\,M_\odot$ the size limit is $R_{\rm eff}=1$ kpc, and for $M_*=10^{11}\,M_\odot$ the size limit is $R_{\rm eff}=1.6$ kpc. The number density first increases with cosmic time, reaching a plateau at $z\sim1.5$–2, after which it strongly decreases toward the present day. The immediate implication is that individual galaxies must grow in size significantly, most likely through merging.

(A color version of this figure is available in the online journal.)

impressive body of evidence for rapid evolution (Zirm 2007; Toft et al. 2007; van Dokkum et al. 2008; Buitrago et al. 2008), later confirmed by *HST*/WFC3-based studies (e.g., Newman et al. 2012; Cassata et al. 2013; Morishita et al. 2014).

What has so far remained contentious is what drives this evolution: the size evolution of individual galaxies, the addition of larger galaxies to the population, or a combination of both. Figure 11 (top panel) shows the cumulative size histograms of early-type galaxies in the L^* mass range, which reveal that the number density of small early-type galaxies strongly evolves with redshift. The total number density of early-type galaxies increases from $z\sim3$ to the present, but the number of small galaxies strongly decreases at late cosmic times. We show this explicitly in Figure 13: the number density of high-mass galaxies with small sizes increases from early times to $z\sim2$, levels off, and then decreases strongly at $z\lesssim1.5$. The definition of small is arbitrary, but the general picture does not depend on the precise choice in mass and size range. This finding is in general agreement with previous claims based on smaller samples and fewer fields by Cassata et al. (2011), Newman et al. (2012), Szomoru et al. (2012), Buitrago et al. (2013), and Cassata et al. (2013).

Several authors have argued that there are a substantial number of small yet massive galaxies in the present-day universe (Valentinuzzi et al. 2010; Poggianti et al. 2013). The latter show that 3%–5% of present-day group and cluster early-type galaxies with mass $M_*>3\times10^{10}\,M_\odot$ can be classified as "compact." Following their definition ($M_*/(2\pi R_{\rm eff,circ})>3\times10^9 M_\odot\,{\rm kpc}^{-2}$), we find that ~40%–50% of $z\sim1$ early-type galaxies qualify as compact. Since the total number density of such galaxies has evolved by no more than a factor two or three, we conclude that most of the $z\sim1$ compact galaxies no longer exist in that form in the present-day universe. Several "fossils" in the form of $R_{\rm eff}\sim1$ kpc, $M_*\sim10^{11}\,M_\odot$ galaxies are found in the local volume (see, e.g., van den Bosch et al.

2012; Dullo & Graham 2013, for recent examples), but their number density is too low to match the number density of their $z = 2$ counterparts.

Recently, Carollo et al. (2013) claimed that the number density of small early-type galaxies in the L^* mass range has not strongly evolved since $z \sim 1$. We rule out that field-to-field variations explain the discrepancy with our results. All five fields show a decline in the number density of compact galaxies (as defined in Figure 13, with $R_{\rm eff} < 2.5$ at $10^{11}\,M_\odot$) between $z = 1.5$ and $z = 0.5$, by factors ranging from 3 to 10. A decline of more than a factor two between $z = 1$ and $z = 0.5$ is seen for four out of five fields.

There are several factors, in the form of systematic effects in the size and mass measurements, that may contribute to this tension. Slight redshift-dependent shifts in the stellar mass estimates produce changes in the size distribution as measured at a fixed mass. Our stellar mass estimates for luminous early-type galaxies have been demonstrated to show small, if any, shifts ($\lesssim$0.1 dex) compared with dynamical mass measurements over the redshift range $0 < z < 2$ (van de Sande et al. 2013; Bezanson et al. 2013; Belli et al. 2014). In addition, our color-gradient correction would introduce a 14% shift of $z = 1$ sizes relative to $z = 0.2$ sizes in the Carollo et al. sample.

Most importantly, the size measurements used here and by Carollo et al. (2013) are obtained with fundamentally different techniques: here we use parameterized profile fits, while Carollo et al. use growth curves. The growth curve method does not take the PSF into account at the time of measurement, but it relies on *a posteriori* correction. The magnitude of the correction depends on the intrinsic structural properties and is inferred from simulated size measurements. For example, galaxies with measured sizes of $\sim$0.″2 receive a negligible correction, whereas galaxies with measured sizes of $\sim$0.″1 receive a factor of 2 correction downward (see Figure 2 of Carollo et al.). With such strongly size-dependent corrections it is difficult to reconstruct the true size distribution, especially when those corrections are of a similar magnitude as the sizes themselves.

In an explicit example in which we apply a systematic, redshift-dependent shift in $R_{\rm eff}$ of order 0.1–0.2 dex per unit redshift we infer non-evolution in the number density of compact galaxies. Given this sensitivity to small shifts in size, we argue that our measurements, which do not require systematic size corrections of more than a few percent (see Section 2.5 and van der Wel et al. 2012), represent the size distribution with good fidelity across the examined redshift range.

5. DISCUSSION

5.1. Evolution of Late-type Galaxies

Remarkably, the observed pace of size evolution for late-type galaxies is essentially the same as the evolution of the dark matter halo radius at a fixed mass, $R \propto H(z)^{-2/3}$, but only when the halo mass and radius are defined with respect to the critical density. In a ΛCDM universe, if halo mass is parameterized with respect to matter density or virial density (assuming top-hat collapse), then Λ causes strong departures from a power law at late cosmic times. The average evolution between $z = 2$ and the present is $R \propto H(z)^{-1.06}$ or $\propto H(z)^{-1.24}$, respectively (Peebles 1980).

The interpretation of such a comparison is not straightforward. However, our novel measurement of the slope and scatter of the size–mass relation provides new constraints. The intrinsic scatter in galaxy size remains approximately the same at all redshifts ($\sim$0.16–0.19 dex, see Figure 6) and is comparable to, but perhaps somewhat smaller than, the scatter of 0.25 dex in the halo spin parameter (e.g., Macciò et al. 2008). This strongly suggests that at all redshifts the sizes of late-type galaxies are set by their dark matter halos, and it encourage us to examine the relation between galaxy sizes and halo properties further.

The power law fits presented in Section 3.1 imply that there is very little or no evolution in the slope of the size–mass relation; it remains flat, $\alpha \equiv d \log R_{\rm eff}/d \log M_* = 0.22 \pm 0.03$, at all redshifts $0 < z < 3$ (Figure 6, middle panel). As argued by Shen et al. (2003), the flat slope suggests that the ratio between galaxy mass and halo mass is not a constant: if it were, the size–mass relation would be steeper ($\alpha = 1/3$) than observed. The underlying assumption is that galaxy size is proportional to halo size (Kravtsov 2013), which we here take to be the case for late-type galaxies. Following Shen et al. (2003), we use the observed slope ($\alpha \sim 1/5$) to constrain the galaxy mass–halo mass relation and find $m_g \equiv M_{\rm gal}/M_{\rm halo} \propto M_{\rm halo}^{\gamma \sim 2/3}$. The observation that the slope of the size–mass relation does not evolve with redshift provides a very stringent constraint on the models: unless a combination of factors conspire to keep this slope constant, the most straightforward explanation is that the slope of the relation between galaxy and halo mass (γ) is similar across the redshift range considered here.

Indeed, entirely independent estimates of the relationship between galaxy and halo mass, based on clustering measurements and abundance matching techniques, provide strong evidence that m_g depends on halo mass, similarly so at different redshifts (e.g., Conroy & Wechsler 2009; Moster et al. 2010; Behroozi et al. 2010; Wake et al. 2011; Moster et al. 2013; Behroozi et al. 2013a). In fact, the most recent studies found that $\gamma = 2/3$ for halos in the mass range $M_{\rm halo} \sim 10^{11-12} M_\odot$, in agreement with what we infer on the basis of the slope of the size–mass relation. In addition, Moster et al. (2013) and Behroozi et al. (2013a) showed that m_g peaks at a similar halo mass ($\sim 10^{12} M_\odot$) at all redshifts $z \lesssim 2$, at around a constant value of $m_g \sim 0.05$. The implication is that m_g does not strongly evolve over the (rather narrow) halo mass range $10^{11-12} M_\odot$ (Behroozi et al. 2013b).

It is unclear whether the observed pace of galaxy size evolution ($R_{\rm eff} \propto H(z)^{-2/3}$) implies that $R_{\rm eff}$ evolves in proportion to $R_{\rm halo}$, as may be expected in the case that galaxy size scales with halo size in the present-day universe (Kravtsov 2013). It may be a coincidence that the observed pace of evolution is the same as that for halo radii with respect to the critical density, and it appears more natural to expect galaxy sizes to scale with halo mass and radius that are defined in terms of matter or virial density. In this spirit, the tendency for late-type galaxies to display rather slower size evolution than expected has been given ample attention in the literature.

Somerville et al. (2008) argued that because halos are less concentrated at high redshift, baryonic disks are larger in proportion to the virial radii of halos, leading to slower size evolution. In addition, Dutton et al. (2011) showed that accreting, gaseous disks with a simple but self-consistent prescription for star formation lead to similarly slow evolution of the stellar disk scale radius as a result of recycling of gas and radial variations in star formation. In addition, stellar feedback may have a more direct impact on disk sizes as low-angular momentum material is ejected (e.g., Maller & Dekel 2002; Brook et al. 2011).

The sizes we measured are the not strictly disk scale lengths, as we sample the whole galaxy, including the bulge. Therefore, bulge formation in late-type galaxies slows down size evolution as parameterized here. Bulge formation can either occur rapidly,

through mergers (Toomre & Toomre 1972) or clump formation and migration in unstable disks (Dekel et al. 2009; Ceverino et al. 2010), or gradually, through secular evolution driven by non-axisymmetries in the disk potential (Kormendy & Kennicutt 2004). The prediction of any of these scenarios is that the galaxies with higher global Sérsic indices will have smaller sizes at a given mass. The observation that evolution is faster at $z > 2$ and slower at $z < 1$ (see Section 4.1 and Figure 12), combined with the appearance of redder, more compact galaxies at late cosmic times, suggests that bulge formation plays an important role in the evolution of half-light radii of late-type galaxies.

5.2. Evolution of Massive Early-type Galaxies

The comoving number density of L^* early types has strongly increased over the redshift range examined in this paper ($0 < z < 3$), as was shown by, e.g., Bell et al. (2004); Faber et al. (2007); Brown et al. (2007); Ilbert et al. (2010); Brammer et al. (2011); Buitrago et al. (2013); Muzzin et al. (2013). Here this is illustrated in Figures 10 and 11. Naturally, the progenitors of the newly formed early-type galaxies must be looked for among the star-forming, late-type population. The skewed size distribution of late types toward small sizes (see Section 3.3 and Figure 10) points at the existence of a population of small late-type galaxies that span the entire size range seen for early-type galaxies. Figure 11 illustrates that this is the case over essentially the entire redshift range probed by our sample.

The tail of small star-forming galaxies shown in Figure 11 at $z > 1.5$ (also see Barro et al. 2013a; Williams et al. 2014; Barro et al. 2013b) may reflect the intriguing possibility of a scenario in which such small yet massive star-forming galaxies are the immediate progenitors of compact early-type galaxies. Their number density does not rapidly change between $z = 3$ and $z = 1.5$, whereas the number of early-type galaxies does rapidly increase over that redshift range (see Figure 11). This would suggest the continuous emergence of additional small late-type galaxies that represent a transitional phase between the bulk of the late-type population and the early-type population, as recently advocated by Dekel & Burkert (2014) on the basis of analytical arguments and simulations.

An alternative interpretation is that the star-forming population consists of "normal" late types and a population of early-type galaxies that revived their star-formation activity. The simplest implementation of this model, in which these "frosting" early types have the same size distribution as the quiescent early types, can be ruled out: the skewed size distribution of late types is not well described by two log-normal distributions centered at the respective peaks of the size distributions for late- and early-type galaxies. In general, the size distribution of the full population of galaxies (early and late types combined) is not observed to be bimodal in the sense that there is no clear gap between two fiducial populations of small and large galaxies, nor can the size distribution be accurately represented by a single Gaussian distribution. More complicated models of the "frosting" flavor, in which a large star-forming disk reassembles to surround a compact, quiescent component, cannot be immediately ruled out. However, such scenarios seem implausible as the implied color and mass-to-light ratio gradients of such galaxies would likely be stronger than observed (Wuyts et al. 2012). Measurements of the stellar density in the central regions of early- and late-type galaxies can be used to provide further constraints.

Whether or not the small late-type galaxies represent a transitional phase, the central idea in the formation of early-type galaxies is that the formation of an early-type galaxy requires the formation of a concentrated stellar body with a high density (e.g., Franx et al. 2008; Bell et al. 2012). One possibility is that a substantial amount of material flows to the center under the influence of mergers (e.g., Di Matteo et al. 2005) or violently unstable disks and clump formation/migration (Dekel et al. 2009; Ceverino et al. 2010; Dekel & Burkert 2014). It remains to be seen whether such processes can reproduce the correct stellar density profiles (Wuyts et al. 2010).

As we showed in Section 4.2 and Figures 11 and 13, the number density of small, compact early-type galaxies strongly decreases between $z \sim 1.5$ and the present. This immediately implies that early-type galaxies, after they first form as compact, quiescent objects, have to substantially grow in size over time. Combining this with the suggestion that new early-type galaxies likely form out of the smallest late-type galaxies, the implication is that early-type galaxies are the most dense (and disklike in structure, e.g., van der Wel et al. 2011; Bruce et al. 2012; Chang et al. 2013) immediately after their star formation is truncated. The amount of later evolution in size and density is dictated by the (non-evolving) slope of the size–mass relation and the evolution of its intercept. This naturally fits into the general idea that a gas-rich formation phase is followed by a more quiescent, dissipationless formation phase.

The scatter in the size–mass relation of ~0.15–0.20 dex (see Figure 6) shows that there is some variation in the amount of dissipative and dissipationless formation, yet the fact that we see little or no evolution in the size scatter, as predicted by Shankar et al. (2013), implies that the amount of dissipation integrated over cosmic history does not vary greatly. Some early-type galaxies may have experienced an intensely dissipative phase at early times, while other—similarly massive—galaxies may have continued a less intense star-forming phase up until recently. The compact $z > 1.5$ early-type galaxies would fall in the former category; the large, massive star-forming galaxies at $z \sim 0.5$–1.5 may be the progenitors of galaxies in the latter.

Within this framework, independent evidence for the increase in stellar mass of individual early-type galaxies by a factor of 2 to 3 between $z = 2$ and the present (van Dokkum et al. 2010) implies that the growth in size depends on the growth in mass as $\Delta R_{\rm eff} \propto \Delta M_*^{\sim 2}$. This steep dependence is consistent with a merger scenario.

Satellite galaxies can be stripped and their stars deposited on large-radius orbits. Direct and stringent constraints on the minor merger rate are difficult to obtain, but it has proved to be difficult to observationally confirm a sufficiently large minor merger rate to explain the observed evolution (Newman et al. 2012). Mergers among galaxies that occupy the size–mass relation for early-type galaxies, that is, pure dry mergers, may not occur at sufficient rates (e.g., Nipoti et al. 2012).

Alternatively, mergers between similarly massive galaxies with different sizes can induce large changes in the size–mass distribution of the population. Assuming that the size distribution of progenitors partaking in major mergers is the same as that of the population as a whole, a $R_{\rm eff} = 1$ kpc early-type galaxy at $z \sim 2$ will merge, on average, with a late-type galaxy that is 3 times larger. The properties of the merger remnant will depend on the amount of dissipation and the dynamics of the merger, but it is conceivable that the remnant will be much larger than the compact progenitor. A dense inner region will remain in place, and the strong correlation between central density and quiescence implies that the remnant is likely to be quiescent as well.

The mass ratio distribution in the merger history of early-type galaxies, and its effect on size evolution, will remain a topic of debate. However, merging can account for, and is arguably required to explain, the disappearance from $z \sim 2$ to the present of disklike structures among L^* early types (van der Wel et al. 2011; Bruce et al. 2012; Chang et al. 2013) and the observation that the most massive galaxies in the present-day universe do not have a disklike structure but are intrinsically round (van der Wel et al. 2009b). A combined analysis of the evolution of size and morphological properties (see, e.g., Huertas-Company et al. 2013) will aid to simultaneously interpret size growth and disk destruction.

The above narrative shows that we have gathered a plausible set of mechanisms that may play a role in explaining the formation and subsequent evolution of early-type galaxies. Despite this, we lack the basis of a simple analytical framework that is similar to our model for disk formation. However, we note that the rapid pace of size evolution is very close to the size evolution expected for halos as defined by their virial density: $R \propto H(z)^{-1.24}$ for halos compares well with $R_{\rm eff} \propto H(z)^{-1.29}$ for massive early-type galaxies. If we assume that these galaxies only grow through the accretion of other halos and their stellar content, then it is perhaps not a coincidence that halos and galaxies both follow the evolutionary path expected for a dissipationless, top-hat collapse scenario.

5.3. Evolution of Low-mass Early-type Galaxies

As we noted in Section 3.2, the slope of the size–mass relation for early-type galaxies flattens below stellar mass $\sim 10^{10}\,M_\odot$, and the size evolution is more comparable to that of late types than that of early types (see Figure 9). This suggests that there is a population of low-mass early types that may have formed out of late-type galaxies without going through a transitional phase in which high central densities are attained. The stripping of gas from satellite galaxies is a natural explanation for such evolution and can explain the existence of an excess population of early-type galaxies in clusters that have structural properties similar to those of late-type galaxies in the field (van der Wel et al. 2010). Satellites are common in this mass range in the present-day universe (e.g., van den Bosch et al. 2008), but not at higher redshifts, lending the stripping scenario more credence on the basis of the rapid increase in the comoving number density since $z \sim 1$–1.5 (see Figures 5 and 10).

On the other hand, the early types with mass $\lesssim 10^{10}\,M_\odot$ are $\sim$2 times smaller than equally massive late types. Disk fading may contribute to this difference, but bulge formation and, in general, processes that cause more massive galaxies to transform into early-type galaxies may play a role in the low-mass regime as well. A model such as that presented by Peng et al. (2010) can be expanded in order to separately reproduce the size–mass relations for different types of "quenched" galaxies.

6. SUMMARY

In this paper we present the size–mass distribution of 30,958 galaxies over a large range in mass ($>10^9\,M_\odot$) and redshift ($0 < z < 3$), distinguishing between early-type and late-type galaxies on the basis of their star-formation activity. Spectroscopic and photometric redshifts, stellar masses, and rest-frame properties are determined by using data from the 3D-HST survey and auxiliary, multiwavelength photometric data sets spanning from the U band to 8 μm (see Section 2). Galaxy sizes are measured from CANDELS imaging by single-component Sérsic profile fits to two-dimensional light distributions, with a correction for (redshift-dependent) color gradients (Section 2.5).

Consistent with previous results, we find that high-redshift galaxies are substantially smaller than equally massive, present-day counterparts. As is shown in Figures 5, 6, and 9, late-type galaxies are, on average, a factor of $\sim$2 smaller at $z = 2$ than at the present day, whereas for massive early-type galaxies this is a factor of $\sim$4. We find that the size evolution of late-type galaxies is marginally better described as a function of the redshift-dependent Hubble parameter, $H(z)$, than as a function of the scale factor, $1 + z$ (Figure 7). Average mass-matched sizes of late- and early-type galaxies evolve as $R_{\rm eff} \propto H(z)^{-0.66} \propto (1+z)^{-.75}$ and $R_{\rm eff} \propto H(z)^{-1.29} \propto (1+z)^{-1.48}$, respectively (Figure 6 and Table 1).

High-mass late-type galaxies evolve marginally faster than low-mass late-type galaxies (Figure 9 and Table 2), but the data are consistent with no evolution in the overall slope of the size–mass relation. At all redshifts $z \leqslant 3$ we find that the slope is shallow for late-type galaxies ($R_{\rm eff} \propto M_*^{0.22}$ for galaxies with stellar mass $M_* > 3 \times 10^9 M_\odot$) and is steep for early-type galaxies ($R_{\rm eff} \propto M_*^{0.75}$ for galaxies with stellar mass $M_* > 2 \times 10^{10} M_\odot$). The size–mass relation for lower-mass early-type galaxies is more similar to that of late types than that of high-mass early types (Section 5.3). Once cross-contamination between the two classes of galaxies and outliers are taken into account (Figure 6 and Section 3.1), we also find no evidence for evolution in the (intrinsic) size scatter at a fixed galaxy mass. The implications of these results are discussed in Section 5.

The data presented here are consistent with essentially most published data sets (Section 4). Because of the sample size and dynamic range in mass and redshift, the immediate implications of the measurements are less ambiguous than was the case for previous studies. In particular, we show in Figure 11 that the size distribution of $z \sim 2$ early-type galaxies is significantly different from that of any subset of low-redshift galaxies with the same comoving number density; small early-type galaxies, which are typical at $z \sim 2$, do not exist in equal numbers today (Figure 13) and must therefore undergo strong size evolution in the intervening time.

The size–mass distributions from the 3D-HST and CANDELS projects presented here provide a solid framework for galaxy evolution models and strongly constrain the interplay between structure formation and galaxy formation (e.g., Stringer et al. 2014). The steadily evolving intercept of the size–mass relation, in combination with the non-evolving slope and scatter, present tight constraints on how baryons condense and form galaxies at the centers of dark matter halos (e.g., Section 5.1). The different assembly mechanisms of early- and late-type galaxies act similarly at all redshifts, as evidenced by the very different but unchanging slopes of their respective size–mass relations.

This work is based on observations taken by the CANDELS Multi-Cycle Treasury Program with the NASA/ESA *HST*, which is operated by the Association of Universities for Research in Astronomy, Inc., under NASA contract NAS5-26555.

APPENDIX

COMPLEMENTARY SIZE DISTRIBUTIONS

Throughout this paper, we use the radius $R_{\rm eff}$ as measured along the major axis. Circularized sizes ($R_{\rm eff,circ} = R_{\rm eff}\sqrt{b/a}$,

Table 3
Logarithmic Size Distribution (16%–84% Range) as a Function of Galaxy Mass and Redshift

		Early-type Galaxies					Late-type Galaxies				
z		$M_* = 10^{9.25}$	9.75	10.25	10.75	11.25	9.25	9.75	10.25	10.75	11.25
	16%	-0.07 ± 0.08	-0.05 ± 0.04	0.02 ± 0.03	0.29 ± 0.04	...	0.07 ± 0.01	0.21 ± 0.02	0.27 ± 0.02	0.51 ± 0.03	...
0.25	50%	0.17 ± 0.01	0.17 ± 0.03	0.24 ± 0.04	0.57 ± 0.03	0.72 ± 0.07	0.30 ± 0.01	0.42 ± 0.01	0.49 ± 0.03	0.70 ± 0.02	0.91 ± 0.04
	84%	0.31 ± 0.03	0.39 ± 0.05	0.48 ± 0.04	0.84 ± 0.05	1.01 ± 0.11	0.54 ± 0.01	0.62 ± 0.02	0.73 ± 0.02	0.86 ± 0.05	1.06 ± 0.06
	16%	-0.11 ± 0.04	-0.25 ± 0.02	-0.11 ± 0.02	0.11 ± 0.02	0.57 ± 0.02	0.04 ± 0.01	0.17 ± 0.01	0.27 ± 0.01	0.39 ± 0.01	0.64 ± 0.04
0.75	50%	0.12 ± 0.02	0.10 ± 0.02	0.13 ± 0.02	0.36 ± 0.01	0.74 ± 0.03	0.26 ± 0.00	0.39 ± 0.01	0.49 ± 0.01	0.61 ± 0.02	0.82 ± 0.03
	84%	0.34 ± 0.02	0.34 ± 0.03	0.33 ± 0.01	0.56 ± 0.01	0.93 ± 0.04	0.47 ± 0.01	0.58 ± 0.01	0.66 ± 0.01	0.78 ± 0.01	0.98 ± 0.02
	16%	...	-0.21 ± 0.02	-0.23 ± 0.01	-0.07 ± 0.02	0.32 ± 0.04	-0.05 ± 0.01	0.10 ± 0.01	0.23 ± 0.01	0.36 ± 0.01	0.51 ± 0.01
1.25	50%	...	0.06 ± 0.03	-0.01 ± 0.02	0.16 ± 0.02	0.49 ± 0.03	0.19 ± 0.00	0.32 ± 0.00	0.42 ± 0.00	0.53 ± 0.01	0.67 ± 0.02
	84%	...	0.33 ± 0.03	0.27 ± 0.03	0.44 ± 0.03	0.75 ± 0.03	0.41 ± 0.01	0.51 ± 0.01	0.60 ± 0.01	0.69 ± 0.01	0.83 ± 0.01
	16%	...	-0.12 ± 0.06	-0.36 ± 0.02	-0.14 ± 0.02	0.11 ± 0.06	-0.09 ± 0.01	0.02 ± 0.01	0.16 ± 0.01	0.24 ± 0.02	0.41 ± 0.03
1.75	50%	...	0.12 ± 0.04	-0.05 ± 0.04	0.08 ± 0.02	0.37 ± 0.03	0.15 ± 0.00	0.24 ± 0.01	0.38 ± 0.01	0.47 ± 0.01	0.58 ± 0.02
	84%	...	0.36 ± 0.04	0.27 ± 0.04	0.42 ± 0.03	0.67 ± 0.03	0.36 ± 0.01	0.46 ± 0.01	0.55 ± 0.01	0.64 ± 0.01	0.75 ± 0.02
	16%	...	...	-0.53 ± 0.09	-0.34 ± 0.03	0.02 ± 0.05	...	-0.06 ± 0.01	0.06 ± 0.02	0.16 ± 0.02	0.29 ± 0.04
2.25	50%	...	...	-0.12 ± 0.05	-0.02 ± 0.03	0.25 ± 0.05	...	0.17 ± 0.01	0.29 ± 0.01	0.39 ± 0.01	0.52 ± 0.02
	84%	...	...	0.25 ± 0.03	0.41 ± 0.06	0.72 ± 0.12	...	0.38 ± 0.01	0.49 ± 0.01	0.56 ± 0.01	0.70 ± 0.02
	16%	...	...	...	-0.37 ± 0.05	-0.08 ± 0.11	...	...	0.01 ± 0.02	0.08 ± 0.05	0.24 ± 0.03
2.75	50%	...	...	...	-0.01 ± 0.04	0.29 ± 0.09	...	...	0.27 ± 0.01	0.34 ± 0.01	0.43 ± 0.02
	84%	...	...	...	0.40 ± 0.06	0.62 ± 0.10	...	...	0.48 ± 0.02	0.54 ± 0.02	0.63 ± 0.06

Note. Identical to Table 2 but with circularized sizes instead of semi-major axis sizes.

Table 4
Logarithmic Size Distributions (16%–84% Range) as a Function of Rest-frame V-band Luminosity and Redshift

		Early-type Galaxies					Late-type Galaxies				
z		$L_* = 10^{9.25}$	9.75	10.25	10.75	11.25	9.25	9.75	10.25	10.75	11.25
	16%	0.04 ± 0.05	0.06 ± 0.03	0.21 ± 0.05	0.61 ± 0.07	...	0.16 ± 0.03	0.31 ± 0.02	0.42 ± 0.02	0.68 ± 0.06	...
0.25	50%	0.27 ± 0.02	0.28 ± 0.02	0.45 ± 0.02	0.72 ± 0.03	...	0.42 ± 0.02	0.57 ± 0.01	0.69 ± 0.02	0.92 ± 0.03	...
	84%	0.44 ± 0.04	0.51 ± 0.04	0.72 ± 0.05	0.99 ± 0.06	...	0.64 ± 0.02	0.76 ± 0.01	0.87 ± 0.02	1.07 ± 0.04	...
	16%	-0.01 ± 0.05	-0.08 ± 0.03	0.05 ± 0.02	0.31 ± 0.01	0.54 ± 0.05	0.06 ± 0.02	0.21 ± 0.01	0.37 ± 0.01	0.54 ± 0.01	0.73 ± 0.10
0.75	50%	0.24 ± 0.02	0.21 ± 0.02	0.27 ± 0.02	0.54 ± 0.02	0.81 ± 0.06	0.33 ± 0.01	0.46 ± 0.01	0.60 ± 0.01	0.75 ± 0.01	0.93 ± 0.08
	84%	0.41 ± 0.02	0.46 ± 0.02	0.47 ± 0.02	0.81 ± 0.02	1.03 ± 0.06	0.57 ± 0.02	0.67 ± 0.00	0.79 ± 0.01	0.93 ± 0.02	1.12 ± 0.08
	16%	-0.10 ± 0.12	-0.12 ± 0.04	-0.14 ± 0.02	0.07 ± 0.02	0.29 ± 0.03	0.03 ± 0.02	0.11 ± 0.01	0.25 ± 0.01	0.43 ± 0.01	0.48 ± 0.05
1.25	50%	0.19 ± 0.04	0.23 ± 0.03	0.10 ± 0.01	0.32 ± 0.01	0.56 ± 0.03	0.32 ± 0.01	0.37 ± 0.01	0.49 ± 0.01	0.64 ± 0.01	0.75 ± 0.02
	84%	0.45 ± 0.11	0.51 ± 0.03	0.40 ± 0.02	0.58 ± 0.03	0.83 ± 0.04	0.66 ± 0.04	0.60 ± 0.01	0.70 ± 0.00	0.82 ± 0.01	0.96 ± 0.03
	16%	...	-0.04 ± 0.08	-0.19 ± 0.03	-0.11 ± 0.03	0.20 ± 0.03	0.12 ± 0.03	0.05 ± 0.01	0.15 ± 0.01	0.32 ± 0.01	0.37 ± 0.08
1.75	50%	...	0.27 ± 0.03	0.09 ± 0.02	0.15 ± 0.02	0.37 ± 0.02	0.43 ± 0.04	0.32 ± 0.01	0.40 ± 0.01	0.56 ± 0.01	0.70 ± 0.03
	84%	...	0.53 ± 0.05	0.39 ± 0.03	0.50 ± 0.04	0.71 ± 0.04	0.82 ± 0.05	0.58 ± 0.01	0.62 ± 0.01	0.75 ± 0.01	0.87 ± 0.01
	16%	...	...	-0.26 ± 0.11	-0.26 ± 0.03	0.00 ± 0.05	...	0.01 ± 0.04	0.08 ± 0.01	0.20 ± 0.01	0.26 ± 0.06
2.25	50%	...	...	0.08 ± 0.04	0.07 ± 0.04	0.24 ± 0.03	...	0.30 ± 0.03	0.34 ± 0.01	0.44 ± 0.01	0.59 ± 0.02
	84%	...	...	0.35 ± 0.08	0.50 ± 0.05	0.49 ± 0.05	...	0.68 ± 0.06	0.56 ± 0.01	0.65 ± 0.01	0.79 ± 0.03
	16%	...	...	...	-0.27 ± 0.03	0.01 ± 0.05	...	...	0.09 ± 0.01	0.18 ± 0.01	0.26 ± 0.07
2.75	50%	...	...	...	0.03 ± 0.05	0.34 ± 0.09	...	...	0.33 ± 0.02	0.43 ± 0.01	0.54 ± 0.02
	84%	...	...	...	0.42 ± 0.07	0.73 ± 0.08	...	...	0.62 ± 0.04	0.63 ± 0.01	0.75 ± 0.02

where b/a is the projected axis ratio) have often been used in the literature. For this reason we provide the circularized size distributions for the early- and late-type samples in Table 3. We stress that since galaxies are predominantly oblate, that is, disklike, using $R_{\rm eff}$ instead of $R_{\rm eff,circ}$ is more prudent: $R_{\rm eff}$ is (almost) independent of inclination, while $R_{\rm eff,circ}$ depends on the short projected axis, which obviously strongly varies with inclination.

Throughout the paper, we distinguish between late- and early-type galaxies on the basis of star formation activity. For some purposes it may be more useful to work with the size distributions of the full sample, without separating by type. In Table 5 we provide the size distributions of the full sample.

Finally, since stellar mass is a derived model-dependent quantity that is potentially suffering from large systematic errors, one might be interested in galaxy size as a function of luminosity, which is essentially a directly observed quantity. In Tables 4 and 5 we provide the size distributions as a function of rest-frame V-band luminosity.

Table 5
Logarithmic Size Distributions (16%–84% Range) for the Full Population (Early- and Late-type Galaxies Combined) as a Function of Mass and Redshift, and Rest-frame *V*-band Luminosity and Redshift

		Early+Late Type Galaxies									
z		$M_* = 10^{9.25}$	9.75	10.25	10.75	11.25	$L_* = 10^{9.25}$	9.75	10.25	10.75	11.25
	16%	0.21 ± 0.01	0.28 ± 0.02	0.27 ± 0.03	0.49 ± 0.04	...	0.14 ± 0.02	0.26 ± 0.02	0.37 ± 0.01	0.62 ± 0.04	...
0.25	50%	0.46 ± 0.01	0.54 ± 0.02	0.54 ± 0.03	0.75 ± 0.03	...	0.37 ± 0.02	0.53 ± 0.01	0.62 ± 0.02	0.79 ± 0.03	...
	84%	0.69 ± 0.01	0.77 ± 0.02	0.82 ± 0.02	0.99 ± 0.02	...	0.62 ± 0.02	0.74 ± 0.01	0.85 ± 0.01	1.05 ± 0.03	...
	16%	0.16 ± 0.01	0.25 ± 0.01	0.18 ± 0.01	0.35 ± 0.02	0.66 ± 0.02	0.05 ± 0.02	0.18 ± 0.01	0.28 ± 0.01	0.40 ± 0.02	0.62 ± 0.06
0.75	50%	0.41 ± 0.01	0.52 ± 0.01	0.52 ± 0.01	0.59 ± 0.01	0.85 ± 0.01	0.29 ± 0.01	0.44 ± 0.01	0.54 ± 0.01	0.68 ± 0.01	0.83 ± 0.04
	84%	0.64 ± 0.01	0.74 ± 0.01	0.78 ± 0.01	0.84 ± 0.01	1.04 ± 0.02	0.54 ± 0.02	0.66 ± 0.00	0.76 ± 0.01	0.90 ± 0.01	1.04 ± 0.04
	16%	...	0.21 ± 0.01	0.15 ± 0.02	0.23 ± 0.02	0.49 ± 0.03	0.02 ± 0.02	0.10 ± 0.01	0.19 ± 0.01	0.29 ± 0.01	0.36 ± 0.04
1.25	50%	...	0.47 ± 0.01	0.52 ± 0.01	0.57 ± 0.01	0.74 ± 0.02	0.30 ± 0.02	0.36 ± 0.01	0.47 ± 0.01	0.58 ± 0.01	0.67 ± 0.04
	84%	...	0.68 ± 0.01	0.74 ± 0.01	0.80 ± 0.01	0.94 ± 0.02	0.64 ± 0.03	0.60 ± 0.01	0.69 ± 0.01	0.79 ± 0.01	0.91 ± 0.03
	16%	...	0.15 ± 0.01	0.12 ± 0.02	0.09 ± 0.01	0.34 ± 0.02	...	0.05 ± 0.01	0.12 ± 0.01	0.16 ± 0.01	0.22 ± 0.02
1.75	50%	...	0.42 ± 0.01	0.48 ± 0.01	0.48 ± 0.01	0.64 ± 0.03	...	0.32 ± 0.01	0.39 ± 0.01	0.51 ± 0.01	0.51 ± 0.04
	84%	...	0.65 ± 0.01	0.69 ± 0.01	0.74 ± 0.01	0.83 ± 0.02	...	0.58 ± 0.01	0.61 ± 0.00	0.73 ± 0.01	0.83 ± 0.02
	16%	...	...	0.10 ± 0.02	0.03 ± 0.03	0.28 ± 0.03	...	...	0.07 ± 0.01	0.15 ± 0.01	0.10 ± 0.03
2.25	50%	...	...	0.41 ± 0.01	0.45 ± 0.02	0.59 ± 0.03	...	...	0.33 ± 0.01	0.43 ± 0.01	0.45 ± 0.03
	84%	...	...	0.63 ± 0.01	0.68 ± 0.01	0.83 ± 0.02	...	...	0.55 ± 0.01	0.64 ± 0.01	0.74 ± 0.03
	16%	...	...	...	0.01 ± 0.03	0.27 ± 0.06	...	...	...	0.11 ± 0.02	0.12 ± 0.06
2.75	50%	...	...	...	0.43 ± 0.01	0.52 ± 0.03	...	...	...	0.41 ± 0.01	0.52 ± 0.03
	84%	...	...	...	0.65 ± 0.02	0.75 ± 0.04	...	...	...	0.62 ± 0.01	0.74 ± 0.02

REFERENCES

Barden, M., Häußler, B., Peng, C. Y., McIntosh, D. H., & Guo, Y. 2012, MNRAS, 422, 449
Barden, M., Rix, H.-W., Somerville, R.∼S., et al. 2005, ApJ, 635, 959
Barro, G., Faber, S. M., Pérez-González, P. G., et al. 2013a, ApJ, 765, 104
Barro, G., Faber, S. M., Perez-Gonzalez, P. G., et al. 2013b, arXiv:1311.5559
Bédorf, J., & Portegies Zwart, S. 2013, MNRAS, 431, 767
Behroozi, P. S., Conroy, C., & Wechsler, R. H. 2010, ApJ, 717, 379
Behroozi, P. S., Wechsler, R. H., & Conroy, C. 2013a, ApJ, 770, 57
Behroozi, P. S., Wechsler, R. H., & Conroy, C. 2013b, ApJL, 762, L31
Bell, E. F., van der Wel, A., Papovich, C., et al. 2012, ApJ, 753, 167
Bell, E. F., Wolf, C., Meisenheimer, K., et al. 2004, ApJ, 608, 752
Belli, S., Newman, A. B., & Ellis, R. S. 2014, ApJ, 783, 117
Bezanson, R., van Dokkum, P. G., Tal, T., et al. 2009, ApJ, 697, 1290
Bezanson, R., van Dokkum, P. G., van de Sande, J., et al. 2013, ApJL, 779, L21
Brammer, G. B., van Dokkum, P. G., & Coppi, P. 2008, ApJ, 686, 1503
Brammer, G. B., van Dokkum, P. G., Franx, M., et al. 2012, ApJS, 200, 13
Brammer, G. B., Whitaker, K. E., van Dokkum, P. G., et al. 2011, ApJ, 739, 24
Brook, C. B., Governato, F., Roškar, R., et al. 2011, MNRAS, 415, 1051
Brown, M. J. I., Dey, A., Jannuzi, B. T., et al. 2007, ApJ, 654, 858
Bruce, V. A., Dunlop, J. S., Cirasuolo, M., et al. 2012, MNRAS, 427, 1666
Bruzual, G., & Charlot, S. 2003, MNRAS, 344, 1000
Buitrago, F., Trujillo, I., Conselice, C. J., & Häußler, B. 2013, MNRAS, 428, 1460
Buitrago, F., Trujillo, I., Conselice, C. J., et al. 2008, ApJL, 687, L61
Carollo, C. M., Bschorr, T. J., Renzini, A., et al. 2013, ApJ, 773, 112
Cassata, P., Giavalisco, M., Guo, Y., et al. 2011, ApJ, 743, 96
Cassata, P., Giavalisco, M., Williams, C. C., et al. 2013, ApJ, 775, 106
Ceverino, D., Dekel, A., & Bournaud, F. 2010, MNRAS, 404, 2151
Chabrier, G. 2003, PASP, 115, 763
Chang, Y.-Y., van der Wel, A., Rix, H.-W., et al. 2013, ApJ, 762, 83
Cimatti, A., Cassata, P., Pozzetti, L., et al. 2008, A&A, 482, 21
Conroy, C., & Wechsler, R. H. 2009, ApJ, 696, 620
Daddi, E., Renzini, A., Pirzkal, N., et al. 2005, ApJ, 626, 680
Damjanov, I., Abraham, R. G., Glazebrook, K., et al. 2011, ApJL, 739, L44
Dekel, A., & Burkert, A. 2014, MNRAS, 438, 1870
Dekel, A., Sari, R., & Ceverino, D. 2009, ApJ, 703, 785
Di Matteo, T., Springel, V., & Hernquist, L. 2005, Natur, 433, 604
Dullo, B. T., & Graham, A. W. 2013, ApJ, 768, 36
Dutton, A. A., van den Bosch, F. C., Faber, S. M., et al. 2011, MNRAS, 410, 1660
Faber, S. M., Willmer, C. N. A., Wolf, C., et al. 2007, ApJ, 665, 265
Fan, L., Lapi, A., Bressan, A., et al. 2010, ApJ, 718, 1460
Ferguson, H. C., Dickinson, M., Giavalisco, M., et al. 2004, ApJL, 600, L107
Franx, M., van Dokkum, P. G., Förster Schreiber, N. M., et al. 2008, ApJ, 688, 770
Giavalisco, M., Steidel, C. C., & Macchetto, F. D. 1996, ApJ, 470, 189
González, V., Labbé, I., Bouwens, R. J., et al. 2010, ApJ, 713, 115
Grogin, N. A., Kocevski, D. D., Faber, S. M., et al. 2011, ApJS, 197, 35
Guo, Y., Giavalisco, M., Cassata, P., et al. 2011, ApJ, 735, 18
Guo, Y., McIntosh, D. H., Mo, H. J., et al. 2009, MNRAS, 398, 1129
Holden, B. P., van der Wel, A., Rix, H.-W., & Franx, M. 2012, ApJ, 749, 96
Hopkins, P. F., Hernquist, L., Cox, T. J., Keres, D., & Wuyts, S. 2009, ApJ, 691, 1424
Huang, K.-H., Ferguson, H. C., Ravindranath, S., & Su, J. 2013, ApJ, 765, 68
Huertas-Company, M., Mei, S., Shankar, F., et al. 2013, MNRAS, 428, 1715
Ilbert, O., Salvato, M., Le Floc'h, E., et al. 2010, ApJ, 709, 644
Kelvin, L. S., Driver, S. P., Robotham, A. S. G., et al. 2012, MNRAS, 421, 1007
Koekemoer, A. M., Faber, S. M., Ferguson, H. C., et al. 2011, ApJS, 197, 36
Kormendy, J. 1977, ApJ, 218, 333
Kormendy, J., & Kennicutt, R. C., Jr. 2004, ARA&A, 42, 603
Kravtsov, A. V. 2013, ApJL, 764, L31
Kriek, M., van Dokkum, P. G., Franx, M., Illingworth, G. D., & Magee, D. K. 2009a, ApJL, 705, L71
Kriek, M., van Dokkum, P. G., Labbé, I., et al. 2009b, ApJ, 700, 221
Labbé, I., Bouwens, R., Illingworth, G. D., & Franx, M. 2006, ApJL, 649, L67
Laidler, V. G., Papovich, C., Grogin, N. A., et al. 2007, PASP, 119, 1325
Lilly, S., Schade, D., Ellis, R., et al. 1998, ApJ, 500, 75
Macciò, A. V., Dutton, A. A., & van den Bosch, F. C. 2008, MNRAS, 391, 1940
Maller, A. H., & Dekel, A. 2002, MNRAS, 335, 487
Mancini, C., Daddi, E., Renzini, A., et al. 2010, MNRAS, 401, 933
McGrath, E. J., Stockton, A., Canalizo, G., Iye, M., & Maihara, T. 2008, ApJ, 682, 303
Mo, H. J., Mao, S., & White, S. D. M. 1998, MNRAS, 295, 319
Morishita, T., Ichikawa, T., & Kajisawa, M. 2014, ApJ, 785, 18
Mosleh, M., Williams, R. J., Franx, M., et al. 2012, ApJL, 756, L12
Moster, B. P., Naab, T., & White, S. D. M. 2013, MNRAS, 428, 3121
Moster, B. P., Somerville, R. S., Maulbetsch, C., et al. 2010, ApJ, 710, 903
Muzzin, A., Marchesini, D., Stefanon, M., et al. 2013, ApJ, 777, 18
Naab, T., Johansson, P. H., & Ostriker, J. P. 2009, ApJL, 699, L178
Newman, A. B., Ellis, R. S., Bundy, K., & Treu, T. 2012, ApJ, 746, 162
Newman, A. B., Ellis, R. S., Treu, T., & Bundy, K. 2010, ApJL, 717, L103
Nipoti, C., Treu, T., Leauthaud, A., et al. 2012, MNRAS, 422, 1714
Oesch, P. A., Bouwens, R. J., Carollo, C. M., et al. 2010, ApJL, 709, L21
Oser, L., Naab, T., Ostriker, J. P., & Johansson, P. H. 2012, ApJ, 744, 63
Peebles, P. J. E. 1980, The Large-Scale Structure of the Universe (Princeton, NJ: Princeton Univ. Press)
Peng, Y.-j., Lilly, S. J., Kovač, K., et al. 2010, ApJ, 721, 193
Poggianti, B. M., Calvi, R., Bindoni, D., et al. 2013, ApJ, 762, 77

Quadri, R. F., & Williams, R. J. 2010, ApJ, 725, 794
Ravindranath, S., Ferguson, H. C., Conselice, C., et al. 2004, ApJL, 604, L9
Saracco, P., Longhetti, M., & Gargiulo, A. 2011, MNRAS, 412, 2707
Shankar, F., Federico, M., Mariangela, B., et al. 2013, MNRAS, 428, 109
Shen, S., Mo, H. J., White, S. D. M., et al. 2003, MNRAS, 343, 978
Skelton, R. E., Whitaker, K. E., Momcheva, I. G., et al. 2014, arXiv:1403.3689
Somerville, R. S., Barden, M., Rix, H.-W., et al. 2008, ApJ, 672, 776
Sonnenfeld, A., Treu, T., Gavazzi, R., et al. 2013, ApJ, 777, 98
Stockton, A., McGrath, E., Canalizo, G., Iye, M., & Maihara, T. 2008, ApJ, 672, 146
Stringer, M. J., Shankar, F., Novak, G. S., et al. 2014, MNRAS, in press (arXiv:1310.3823)
Szomoru, D., Franx, M., Bouwens, R. J., et al. 2011, ApJL, 735, L22
Szomoru, D., Franx, M., & van Dokkum, P. G. 2012, ApJ, 749, 121
Szomoru, D., Franx, M., van Dokkum, P. G., et al. 2010, ApJL, 714, L244
Taylor, E. N., Franx, M., Glazebrook, K., et al. 2010, ApJ, 720, 723
Toft, S., Gallazzi, A., Zirm, A., et al. 2012, ApJ, 754, 3
Toft, S., Smolčić, V., Magnelli, B., et al. 2014, ApJ, 782, 68
Toft, S., van Dokkum, P., Franx, M., et al. 2007, ApJ, 671, 285
Toomre, A., & Toomre, J. 1972, ApJ, 178, 623
Trujillo, I., Cenarro, A. J., de Lorenzo-Cáceres, A., et al. 2009, ApJL, 692, L118
Trujillo, I., Conselice, C. J., Bundy, K., et al. 2007, MNRAS, 382, 109
Trujillo, I., Feulner, G., Goranova, Y., et al. 2006b, MNRAS, 373, L36
Trujillo, I., Förster Schreiber, N. M., Rudnick, G., et al. 2006a, ApJ, 650, 18
Valentinuzzi, T., Fritz, J., Poggianti, B. M., et al. 2010, ApJ, 712, 226
van de Sande, J., Kriek, M., Franx, M., et al. 2011, ApJL, 736, L9
van de Sande, J., Kriek, M., Franx, M., et al. 2013, ApJ, 771, 85
van den Bosch, F. C., Aquino, D., Yang, X., et al. 2008, MNRAS, 387, 79
van den Bosch, R. C. E., Gebhardt, K., Gültekin, K., et al. 2012, Natur, 491, 729
van der Wel, A., Bell, E. F., Häussler, B., et al. 2012, ApJS, 203, 24
van der Wel, A., Bell, E. F., Holden, B. P., Skibba, R. A., & Rix, H.-W. 2010, ApJ, 714, 1779
van der Wel, A., Bell, E. F., van den Bosch, F. C., Gallazzi, A., & Rix, H.-W. 2009a, ApJ, 698, 1232
van der Wel, A., Franx, M., Wuyts, S., et al. 2006, ApJ, 652, 97
van der Wel, A., Holden, B. P., Zirm, A. W., et al. 2008, ApJ, 688, 48
van der Wel, A., Rix, H.-W., Holden, B. P., Bell, E. F., & Robaina, A. R. 2009b, ApJL, 706, L120
van der Wel, A., Rix, H.-W., Wuyts, S., et al. 2011, ApJ, 730, 38
van der Wel, A., van de Ven, G., Maseda, M., et al. 2013, ApJL, 777, L17
van Dokkum, P. G., Franx, M., Kriek, M., et al. 2008, ApJL, 677, L5
van Dokkum, P. G., Whitaker, K. E., Brammer, G., et al. 2010, ApJ, 709, 1018
Wake, D. A., Whitaker, K. E., Labbé, I., et al. 2011, ApJ, 728, 46
Whitaker, K. E., Labbé, I., van Dokkum, P. G., et al. 2011, ApJ, 735, 86
Williams, C. C., Giavalisco, M., Cassata, P., et al. 2014, ApJ, 780, 1
Williams, R. J., Quadri, R. F., Franx, M., van Dokkum, P., & Labbé, I. 2009, ApJ, 691, 1879
Williams, R. J., Quadri, R. F., Franx, M., et al. 2010, ApJ, 713, 738
Wuyts, S., Cox, T. J., Hayward, C. C., et al. 2010, ApJ, 722, 1666
Wuyts, S., Förster Schreiber, N. M., Genzel, R., et al. 2012, ApJ, 753, 114
Wuyts, S., Labbé, I., Franx, M., et al. 2007, ApJ, 655, 51
Zirm, A. W., van der Wel, A., Franx, M., et al. 2007, ApJ, 656, 66